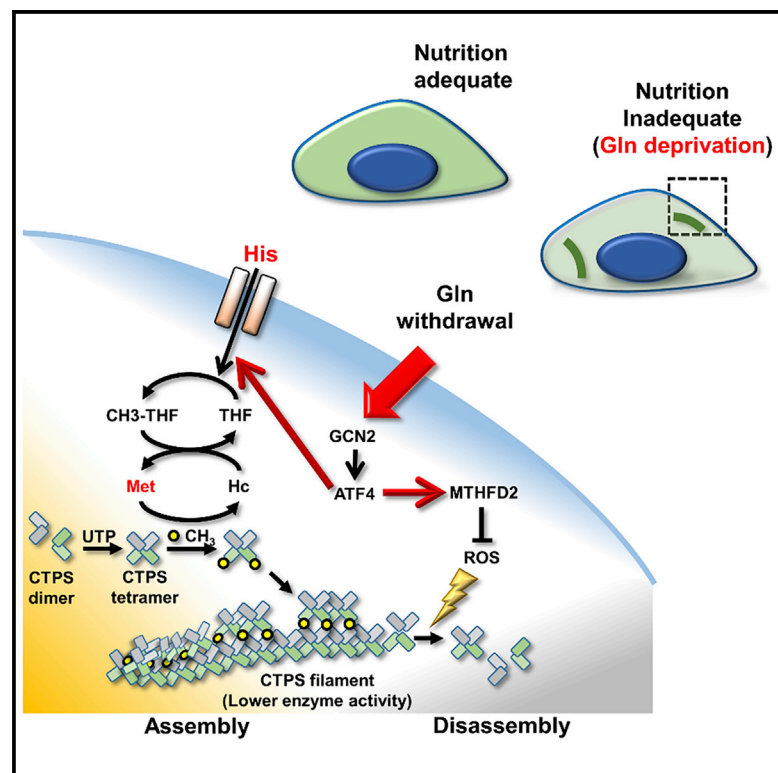


Histidine-Dependent Protein Methylation Is Required for Compartmentalization of CTP Synthase

Graphical Abstract



Authors

Wei-Cheng Lin, Archan Chakraborty, Shih-Chia Huang, ..., Jau-Song Yu, Yu-Sun Chang, Li-Mei Pai

Correspondence

pai@mail.cgu.edu.tw

In Brief

Metabolic enzymes form membraneless compartments to adapt to environmental changes. Lin et al. demonstrate that histidine catabolism coupled with the folate cycle contributes to methionine synthesis, which promotes protein methylation. This post-translational modification in turn induces CTPS filament formation to preserve CTPS but reduces its enzymatic activity under starvation.

Highlights

- Histidine is essential and sufficient for CTPS filament formation during starvation
- The enzymatic activity of CTPS is reduced when it is in a filamentous structure
- The GCN2/ATF4/MTHFD2 stress response pathway coordinates CTPS filament formation
- Histidine-mediated regulation of cytosolic folate cycle promotes protein methylation



Histidine-Dependent Protein Methylation Is Required for Compartmentalization of CTP Synthase

Wei-Cheng Lin,^{2,4} Archan Chakraborty,¹ Shih-Chia Huang,⁷ Pei-Yu Wang,^{2,4} Ya-Ju Hsieh,⁴ Kun-Yi Chien,^{2,18} Yen-Hsien Lee,² Chia-Chun Chang,¹⁰ Hsiang-Yu Tang,^{3,5} Yu-Tsun Lin,² Chang-Shung Tung,¹¹ Ji-Dung Luo,^{4,6} Ting-Wen Chen,^{4,15} Tzu-Yang Lin,^{8,12} Mei-Ling Cheng,^{1,3,5,17} Yi-Ting Chen,^{1,3,4,19} Chau-Ting Yeh,^{1,16} Ji-Long Liu,^{13,14} Li-Ying Sung,^{9,10} Ming-Shi Shiao,^{1,3,5} Jau-Song Yu,^{1,2,4,16} Yu-Sun Chang,^{1,4} and Li-Mei Pai^{1,2,4,16,20,*}

¹Graduate Institute of Biomedical Sciences, College of Medicine, Chang Gung University, Taoyuan 33302, Taiwan

²Department of Biochemistry and Molecular Biology, College of Medicine, Chang Gung University, Taoyuan 33302, Taiwan

³Department of Biomedical Sciences, College of Medicine, Chang Gung University, Taoyuan 33302, Taiwan

⁴Molecular Medicine Research Center, Chang Gung University, Taoyuan 33302, Taiwan

⁵Healthy Aging Research Center, Chang Gung University, Taoyuan 33302, Taiwan

⁶Bioinformatics Core Laboratory, Chang Gung University, Taoyuan 33302, Taiwan

⁷Genomics Research Center, Academia Sinica, Taipei 11529, Taiwan

⁸Institute of Cellular and Organismic Biology, Academia Sinica, Taipei 11529, Taiwan

⁹Agricultural Biotechnology Research Center, Academia Sinica, Taipei 11529, Taiwan

¹⁰Institute of Biotechnology, National Taiwan University, Taipei 106, Taiwan

¹¹Theoretical Biology and Biophysics Group, Los Alamos National Laboratory, Los Alamos, NM 87545, USA

¹²Graduate Institute of Life Sciences, National Defense Medical Center, Taipei 114, Taiwan

¹³Department of Physiology, Anatomy and Genetics, University of Oxford, Oxford OX1 3PT, UK

¹⁴School of Life Science and Technology, ShanghaiTech University, Shanghai 201210, China

¹⁵Departments of Otolaryngology-Head & Neck Surgery, Chang Gung Memorial Hospital, Linkou, Taiwan

¹⁶Liver Research Center, Chang Gung Memorial Hospital, Linkou, Taiwan

¹⁷Clinical Metabolomics Core Laboratory, Chang Gung Memorial Hospital, Linkou, Taiwan

¹⁸Clinical Proteomics Core Laboratory, Chang Gung Memorial Hospital, Linkou, Taiwan

¹⁹Kidney Research Center, Department of Nephrology, Chang Gung Memorial Hospital, Linkou, Taiwan

²⁰Lead Contact

*Correspondence: pai@mail.cgu.edu.tw

<https://doi.org/10.1016/j.celrep.2018.08.007>

SUMMARY

CTP synthase (CTPS) forms compartmentalized filaments in response to substrate availability and environmental nutrient status. However, the physiological role of filaments and mechanisms for filament assembly are not well understood. Here, we provide evidence that CTPS forms filaments in response to histidine influx during glutamine starvation. Tetramer conformation-based filament formation restricts CTPS enzymatic activity during nutrient deprivation. CTPS protein levels remain stable in the presence of histidine during nutrient deprivation, followed by rapid cell growth after stress relief. We demonstrate that filament formation is controlled by methylation and that histidine promotes re-methylation of homocysteine by donating one-carbon intermediates to the cytosolic folate cycle. Furthermore, we find that starvation stress and glutamine deficiency activate the GCN2/ATF4/MTHFD2 axis, which coordinates CTPS filament formation. CTPS filament formation induced by histidine-mediated methylation may be a strategy used by cancer cells to maintain homeo-

stasis and ensure a growth advantage in adverse environments.

INTRODUCTION

The cytoplasm of eukaryotic cells is highly organized, separating specific biochemical and metabolic reactions into membrane-bound organelles. Growing evidence indicates that compartmentalization of metabolic pathways into membraneless organelles is critical for normal cell functions, such as the formation of germline P granules, stress granules, and purinosomes (An et al., 2008; Brangwynne et al., 2009; Hyman et al., 2014; Kedersha et al., 1999; O'Connell et al., 2012).

Cytidine triphosphate (CTP) synthase (CTPS), a critical metabolic enzyme in the *de novo* pyrimidine biosynthetic pathway, can also compartmentalize into filamentous structures in various organisms (Carcamo et al., 2011; Ingerson-Mahar et al., 2010; Liu, 2010; Noree et al., 2010). These compartments assemble dynamically in response to environmental changes (Calise et al., 2014; Chen et al., 2011; Gou et al., 2014; Pai et al., 2016). This catalytic enzyme, with an N-terminal synthetase domain and C-terminal glutamine-dependent amidotransferase (GAT) domain, uses ATP, uridine triphosphate (UTP), and glutamine to produce CTP, necessary for DNA, RNA, and



phospholipid biosynthesis. In human cells, CTPS filaments assemble into rods and rings (RR) in response to glutamine antagonists or glutamine deprivation (Calise et al., 2014; Carcamo et al., 2011; Chen et al., 2011; Gou et al., 2014). The filamentous structures of CTPS have been linked to the regulation of enzymatic activity through steric inhibition associated with nucleotide interactions (Barry et al., 2014; Lynch et al., 2017; Noree et al., 2014). *In vitro* study showed that human CTPS filaments are composed of active UTP-binding tetramers (Lynch et al., 2017). We and others have recently demonstrated that CTPS filament formation is regulated by casitas B-lineage lymphoma (Cbl), and activated cdc42-associated kinase (Ack) and Myc in *Drosophila*, respectively (Aughey et al., 2016; Strohlic et al., 2014; Wang et al., 2015). However, the mechanisms involved in the regulation of CTPS filament formation are still poorly understood.

The crucial role of CTPS has already been studied in various cancer types (Kizaki et al., 1980; van den Berg et al., 1993; Williams et al., 1978). Cancer cells reprogram metabolism to cope with increased energy demands and environmental nutrient availability for physiological homeostasis. Although glutamine is a non-essential amino acid, most cancer cells require an exogenous glutamine supply to meet the large demands of various synthetic pathways and energy production during carcinogenesis driven by active oncogenic genes. General control non-repressible 2 (GCN2)-mediated selective translation of activating transcription factor 4 (ATF4) plays a major role in activating the integrated stress response (ISR) under glutamine depletion (Chen et al., 2014; Harding et al., 2003). Additionally, the reversibility of CTPS filament formation depends on exogenous glutamine availability in human cells (Calise et al., 2014; Gou et al., 2014). Overall, these findings suggest a functional association between CTPS filament formation and stress responses.

Here, we demonstrate that in the absence of glutamine, the supply of essential amino acids induces CTPS filament formation. Unexpectedly, histidine alone was sufficient to induce filament formation. Histidine-induced filament formation required GCN2/ATF4/MTHFD2 axis-mediated redox homeostasis. Inhibition of histidine-dependent protein transmethylation led to impaired filament formation. The filament can reduce enzymatic activity and preserve CTPS for rapid use upon nutrient replenishment. These results provide evidence for the major role of histidine in one-carbon metabolism-mediated transmethylation to regulate CTPS filament formation and may shed light on cancer biology and therapeutic strategies.

RESULTS

Histidine Influx Compartmentalizes CTPS into a Filamentous Structure during Nutrition Deprivation

Glutamine deprivation and glutamine analogs induce the assembly of CTPS filaments in several human cancer cell lines, such as HEP-2, HCT116, and HeLa (Calise et al., 2014; Carcamo et al., 2011; Chen et al., 2011; Gou et al., 2014). Glutamine deprivation has been determined to interfere with intracellular amino acid homeostasis (Chen et al., 2014). We examined the effect of extracellular nutrients on CTPS filament formation by subjecting HEP-2 cells to various nutrient conditions for 24 hr to study the

underlying molecular mechanisms of this phenomenon (Figure 1A). No filaments were formed in complete DMEM or serum-deprived medium. Glutamine deprivation resulted in the formation of CTPS filaments in 3% of treated cells. Additional serum deprivation led to a 40% increase in filament formation. Such conditions may mimic the tumor microenvironment, in which the blood supply might be restricted. However, Earle's balanced salt solution (EBSS), lacking serum, vitamins, and all amino acids (Table S1), induced filament formation in 20% of treated cells. These results suggest that exogenous amino acids, except glutamine, are required for CTPS filament formation.

Amino acid homeostasis is maintained during glutamine/serum deprivation by enhancing the influx of exogenous amino acids through the general amino acid control (GAAC) pathway (Chen et al., 2014). We tested the role of essential amino acids (EAAs) in promoting filament formation by culturing cells in EBSS + EAA. EAA treatment for 24 hr induced filament formation in 70% of cells. We added 2-amino-2-norbornanecarboxylic acid (BCH), which inhibits amino acid transport, to EBSS + EAA or glutamine/serum deprivation media to confirm the effect of amino acid influx (Kim et al., 2008). The number of cells with CTPS filaments decreased in response to BCH treatment under both conditions (Figure 1B). These results indicate that glutamine/serum deprivation induces the influx of exogenous amino acids, thus inducing filament formation.

We assessed which amino acid(s) is or are essential for the formation of CTPS filaments by removing individual amino acids from EBSS + EAA. Strikingly, only histidine withdrawal dramatically reduced filament formation (Figure S1A). We then addressed whether histidine itself could induce filament formation in EBSS. Histidine treatment (EBSS + His) led to filament formation in a dose- and time-dependent manner (Figures 1C). The influx of histidine for the induction of filament formation was confirmed by BCH treatment (Figure S1B). We assessed the role of histidine under physiological conditions by removing it from the glutamine/serum deprivation media. This led to a substantial reduction in CTPS filament formation (Figure 1D). Furthermore, the addition of histidine (200 μ M) to cells cultured for 16 hr in glutamine/serum deprivation media increased CTPS filament formation at 24 hr compared with that without histidine addition (Figure 1D). This result confirms the critical role of histidine in the induction of this process. Furthermore, the filaments disassembled in the presence of glutamine, which is known to disassemble CTPS filaments induced by glutamine deprivation (Calise et al., 2014; Gou et al., 2014) (Figure S1B). In addition, filament formation was also blocked in response to cycloheximide (CHX) treatment (Figure S1B), indicating that new protein synthesis was required. We also observed filament formation in HeLa and U2OS tumor cell lines grown in glutamine/serum deprivation media and EBSS + His (Figure 1E). Thus, we demonstrated that the influx of histidine is required and sufficient for CTPS filament formation during glutamine deprivation.

The Formation of hCTPS Filaments Reduces Enzymatic Activity and Preserves Protein Stability during Nutritional Deprivation

The link between enzymatic activity and CTPS filaments has been determined in *E. coli*, yeast, and humans (Barry et al.,

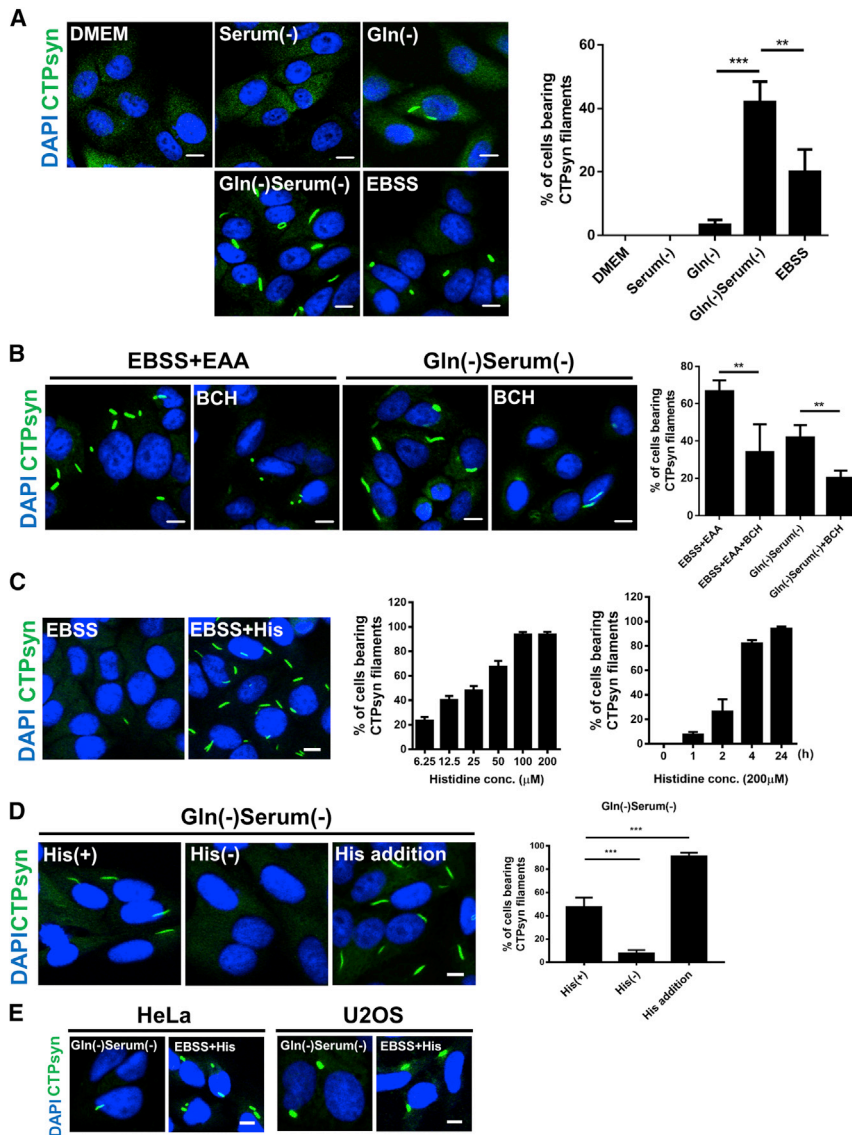


Figure 1. Histidine Is Required for CTPS Filament Formation

(A) HEP-2 cells were incubated with DMEM, serum-negative medium, Gln-negative medium, serum/Gln-negative medium, and EBSS for 24 hr, followed by immunostaining against CTPS (green) and DAPI (blue). Scale bars: 10 μ m.

(B) HEP-2 cells were cultured in serum/Gln-negative medium and EBSS + EAA, with or without BCH (10 mM) treatment, for 24 hr. Cells were stained with anti-CTPS (green) and DAPI (blue). Scale bars, 10 μ m.

(C) HEP-2 cells were incubated in the indicated concentrations of histidine in EBSS for the indicated times, followed by immunostaining against CTPS (green) and DAPI (blue). Scale bar: 10 μ m.

(D) HEP-2 cells were incubated in serum/Gln-negative medium, with or without histidine (His + or His -) for 24 hr. HEP-2 cells were incubated in serum/Gln-negative medium for 16 hr, then added histidine (His addition) for 8 hr. Cells were stained with anti-CTPS (green) and DAPI (blue). Scale bars: 10 μ m.

(E) HeLa and U2OS were incubated in serum/Gln-negative medium for 48 hr or EBSS + His for 24 hr, followed by immunostaining against CTP (green) and DAPI (blue). Scale bar: 10 μ m.

The percentage of cells bearing CTPS filaments was calculated: mean \pm SD, **p < 0.01 and ***p < 0.001.

(Figure S2B), suggesting that the exogenous mutant competed with endogenous wild-type CTPS. The CTP binding mutant (hCTPS1^{E161K}) formed filaments unlike hCTPS1^{G148A} (Figure S2A). As expected, the hCTPS1^{E161K} mutant showed a higher ratio of CTP/UTP than hCTPS1^{WT} (Figure S2B), since CTP could not provide feedback inhibition on the enzymatic activity of this mutant. Both the linker region and GAT domain have been shown to mediate the interaction between tetramers in *E. coli* and humans, respectively (Barry et al., 2014; Lynch et al., 2017). The linker region (hCTPS1^{R294D}) mutant affected filament formation, but the CTP/UTP ratio was similar to that of hCTPS1^{WT} (Figures 2A and S2B), indicating that this mutation interferes with filament formation but not the enzymatic activity of CTPS. Applying this mutant to the cryoelectron microscopy (cryo-EM) modeling of human CTPS filaments suggested that reduced filament formation by CTPS^{R294D} might be due to weakening of the interaction between tetramers (Lynch et al., 2017) (Figure 2B). These results demonstrate that UTP binding and the interface interaction between linker regions are indispensable for filament formation.

Increased catalytic activity of human CTPS in filaments has been demonstrated following *in vitro* assembly in the presence of substrate (Lynch et al., 2017). However, the *in vivo* enzymatic activity of intracellular CTPS in filaments under conditions of nutrient starvation has yet to be investigated. We treated cells

2014; Lynch et al., 2017; Noree et al., 2014). In *E. coli*, the CTPS filaments are stabilized in an inactive tetramer conformation, in contrast to humans, in which the CTPS filaments are stabilized in an active tetramer (Barry et al., 2014; Lynch et al., 2017). We introduced mutations to human CTPS1 (hCTPS1) to assess filament formation and quantified the nucleotide pool under histidine treatment to better understand the conformation and activity of CTPS in filamentous structure formation under conditions of nutrient deprivation. We assessed the CTP/UTP ratio of transfected 293T cells by ultraperformance liquid chromatography (UPLC) analysis to measure the enzymatic activity of exogenous CTPS. The UTP-binding (hCTPS1^{G148A}) mutant could not form filaments (Figure S2A), indicating that substrate binding is required prior to filament formation. This result is consistent with previous findings concerning CTPS filaments of humans (Lynch et al., 2017). The CTP/UTP ratio of hCTPS1^{G148A} transfected cells was significantly lower than that of hCTPS1^{WT}

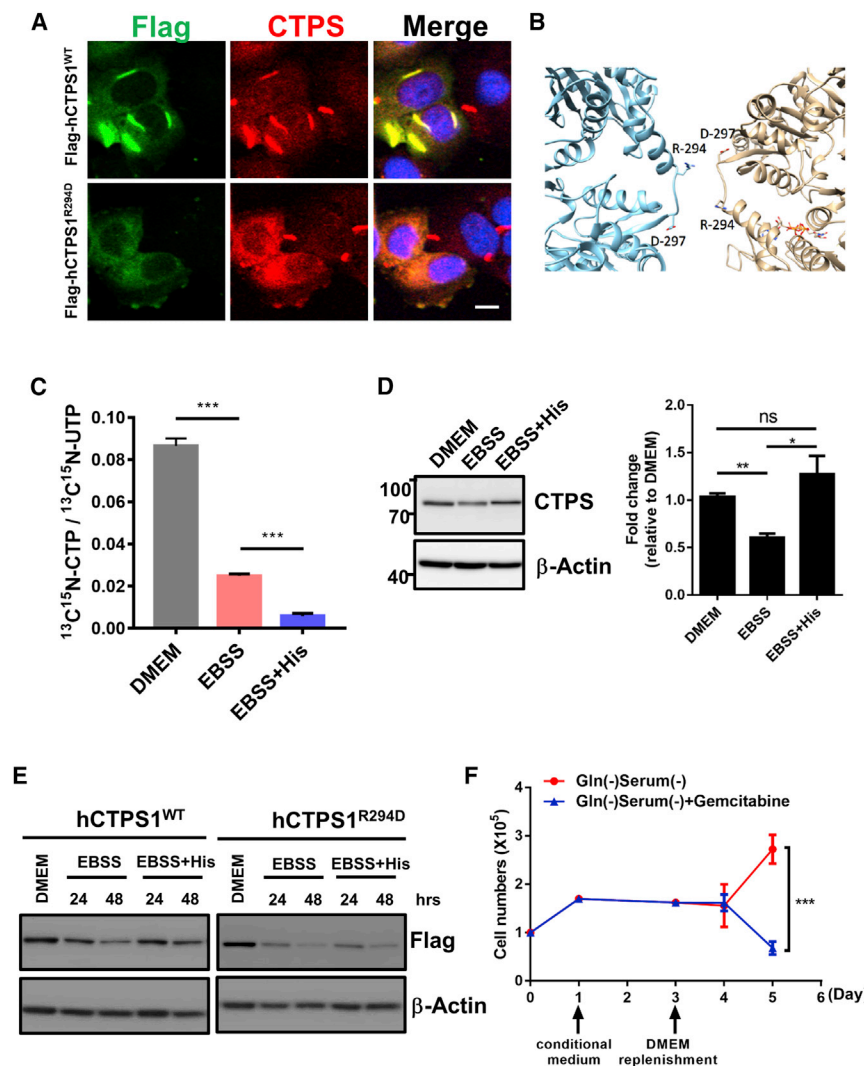


Figure 2. CTPS Filament Formation Down-regulates Enzyme Activity and Maintains Protein Stability

(A) HEp-2 cells expressing exogenous hCTPS1 (hCTPS1^{WT}) and those overexpressing hCTPS1^{R294D} were incubated in EBSS + His for 24 hr, followed by immunostaining against Flag-CTPS (green), CTPS (red), and DAPI (blue). Scale bar: 10 μ m.

(B) Structural modeling showed that residue R294 is close to D297 at the interface between two consecutive tetramers with potential H-bonds.

(C) HEp-2 cells were cultured in DMEM, EBSS, or EBSS + His for 24 hr, followed by treatment with $^{13}\text{C}^{15}\text{N}$ -uridine (100 μ M) for 1 hr. The ratio of labeled CTP to labeled UTP is shown.

(D) HEp-2 cells were incubated in DMEM, EBSS, or EBSS + His for 48 hr. Anti-CTPS and anti-actin antibodies were used for detection by western blotting. Band intensity of CTPS was quantified and normalized against that of actin.

(E) HEp-2 cells expressing exogenous hCTPS1 (hCTPS1^{WT}) and those overexpressing hCTPS1^{R294D} were incubated in DMEM or conditional medium for 24 and 48 hr. Protein levels of Flag-CTPS-transfected cells were evaluated by western blotting.

(F) One hundred thousand cells were seeded at day 0 in DMEM and incubated overnight. DMEM was replaced by serum/Gln-negative medium for 2 days, which were then replaced by DMEM, with or without gemcitabine (100 μ M) treatment. Cells were counted at the indicated times.

Data are presented as mean \pm SD of three independent experiments. ns, not significant; *p < 0.05, **p < 0.01 and ***p < 0.001.

with stable isotope-labeled uridine ($^{13}\text{C}^{15}\text{N}$ -uridine) to trace the incorporation of $^{13}\text{C}^{15}\text{N}$ -uridine into UTP and CTP to evaluate the enzymatic activity of CTPS. The conversion of uridine into UTP could be detected in both EBSS and EBSS + His groups (Figure S2C). The synthesis of CTP in the presence of histidine was significantly lower than that in its absence (Figure 2C), even though the protein levels of CTPS were higher in EBSS + His than EBSS (Figure 2D). This suggests that filament formation not only negatively regulates the enzymatic activity of CTPS but also maintains CTPS protein levels by inducing filament formation. Indeed, CTPS^{R294D} protein, which could not form filaments, was not preserved by histidine treatment in EBSS (Figures 2E and S2D). This mutant demonstrated that proper conformation of the filament is required for protein preservation.

The maintenance of CTPS protein levels by filamentous structures may help meet the high demand of building-block synthesis for cancer cell growth in adverse environments. We tested this possibility by culturing cells with EBSS, with or without histidine, for 48 hr, followed by replacement with DMEM. The rate of cellular proliferation was 3.5-fold higher in cells that were cultured in

EBSS + His than in EBSS alone prior to switch to DMEM by the BrdU incorporation assay (Figure S2E). Cell numbers counted after replace with DMEM increased more quickly in previous culture condition of EBSS + His than that in EBSS alone (EBSS + His: EBSS > 2-fold) (Figure S2F). Treatment with the CTPS inhibitor gemcitabine (McCluskey et al., 2016) substantially reduced cell growth following the addition of DMEM to cells grown in glutamine/serum deprivation and EBSS + His (Figures 2F and S2G). Thus, filament formation positively correlates with cellular proliferation, suggesting that histidine-induced filament formation allows efficient proliferation following nutrient replenishment.

The GCN2/ATF4/MTHFD2 Axis Coordinates CTPS Filament Formation

ATF4 can be induced to switch cellular metabolism, including amino acid influx through GCN2 signaling, to adapt to the fast-ing environment (Chen et al., 2014; Kilberg et al., 2009). Indeed, the levels of most intracellular EAAs increased upon glutamine/serum deprivation (Figure 3A). We thus tested whether histidine-induced CTPS filament formation is regulated by ATF4. ATF4 expression was elevated under conditions of glutamine deprivation, glutamine/serum deprivation, EBSS, and

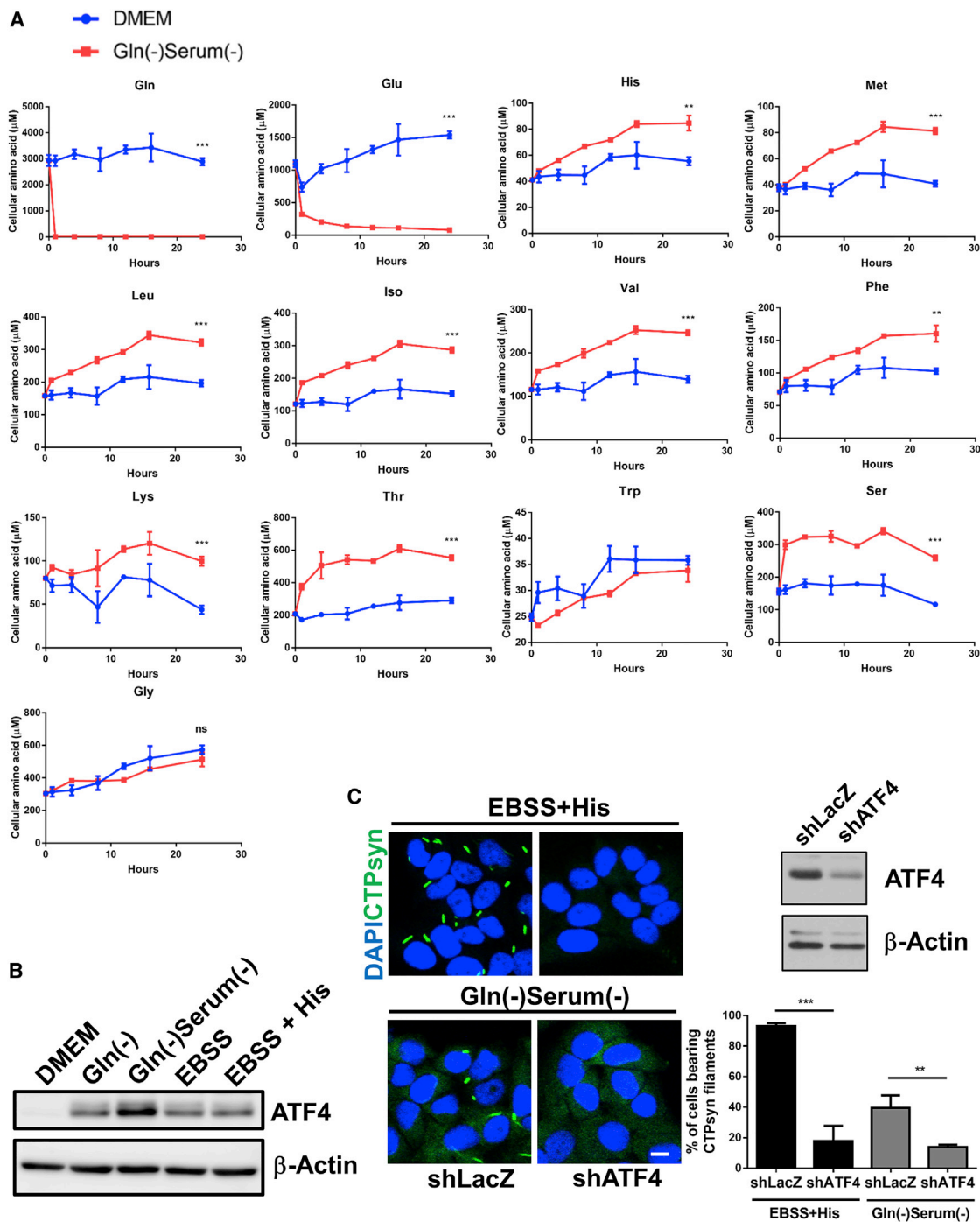


Figure 3. Glutamine Deprivation-Induced Activation of ATF4 Is Indispensable for CTPS Filament Formation

(A) Eight hundred thousand HEP-2 cells were seeded in DMEM and incubated overnight. The culture medium was replaced by serum/Gln-negative medium or DMEM. Amino acid levels were quantified at indicated time points after medium was replaced.

(B) HEP-2 cells were cultured in DMEM, Gln-negative medium, serum/Gln-negative medium, EBSSm or EBSS + His for 4 hr. Anti-ATF4 and anti-actin antibodies were used for detection by western blotting.

(C) The shLacZ and shATF4 stable knockdown cells were incubated in serum/Gln-negative medium or EBSS + His (50 μ M) for 24 hr, followed by immunostaining against CTPS (green) and DAPI (blue). The percentage of cells bearing CTPS filaments was calculated. Scale bar: 10 μ m. ATF4 protein levels were evaluated by western blotting.

Data are presented as mean \pm SD of three independent experiments. **p < 0.01 and ***p < 0.001.

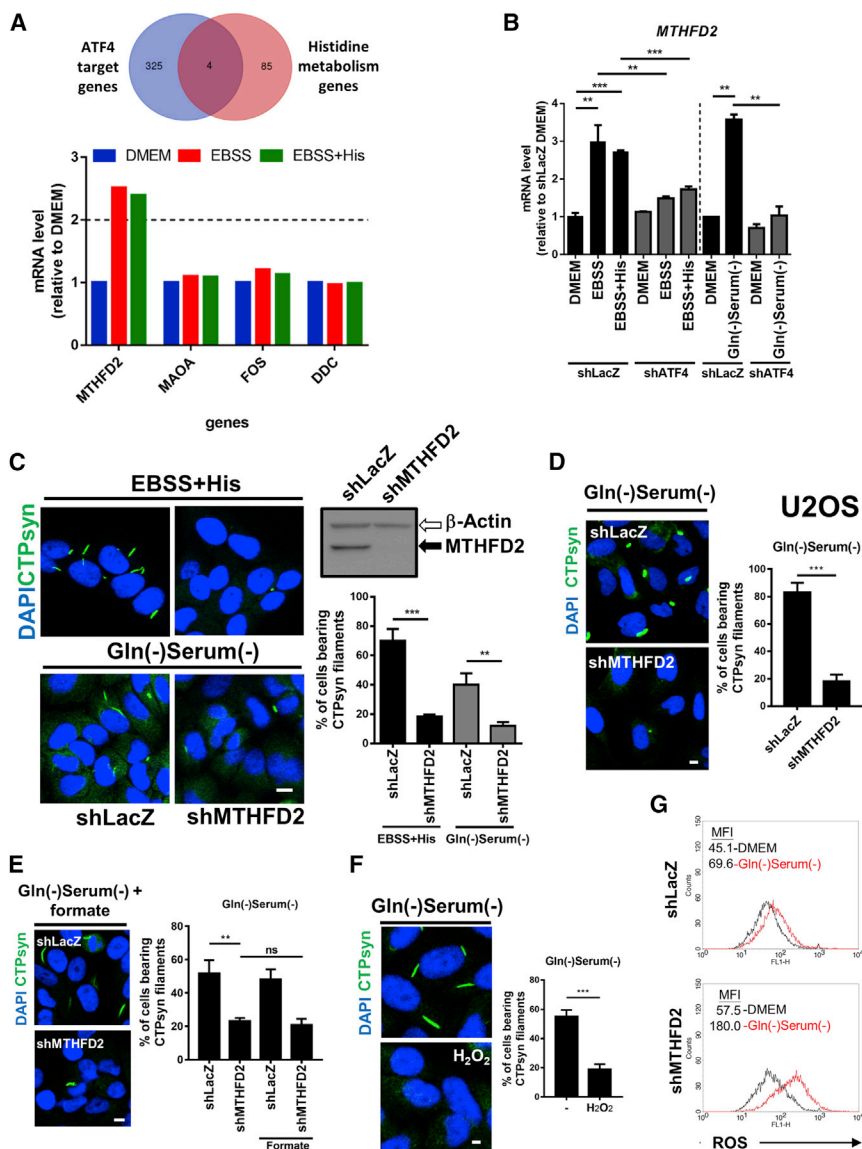


Figure 4. ATF4-MTHFD2 Axis Is Required for CTPS Filament Formation

(A) Venn diagram comparing ATF4 downstream genes with histidine metabolism-related genes.

(B) MTHFD2 mRNA expression was measured in shLacZ and shATF4 stable knockdown cells by qPCR following incubation in DMEM, EBSS, EBSS + His, or serum/Gln-negative medium for 4 hr. The bar graph shows normalized fold expression of MTHFD2 mRNA in conditional medium relative to DMEM. GAPDH was used as an internal control.

(C) The shLacZ and shMTHFD2 stable knockdown cells were incubated in serum/Gln-negative medium or EBSS + His (50 μ M) for 24 hr, followed by immunostaining against CTPS (green) and DAPI (blue). Scale bar: 10 μ m.

(D) The MTHFD2 stable knockdown U2OS cells were incubated in serum/Gln-negative medium for 48 hr, followed by immunostaining against CTPS (green) and DAPI (blue). Scale bar: 10 μ m.

(E) The shLacZ and shMTHFD2 stable knockdown cells were incubated in serum/Gln-negative medium plus formate (1 mM) for 24 hr, followed by immunostaining against CTPS (green) and DAPI (blue). Scale bar: 10 μ m.

(F) HEP-2 cells were incubated in serum/Gln-negative medium for 24 hr, then treated with H₂O₂ (200 μ M) for 1 hr.

(G) The LacZ and MTHFD2 knockdown cells were incubated in DMEM or serum/Gln-negative medium for 24 hr. Intracellular ROS levels stained by 2',7'-dichlorodihydrofluorescein diacetate (DCF-DA) were analyzed by flow cytometry. Data are presented as mean \pm SD of three independent experiments. **p < 0.01 and ***p < 0.001.

EBSS + His (Figure 3B). Knockdown of GCN2 suppressed the upregulation of ATF4, suggesting that glutamine restriction upregulated ATF4 synthesis (Figure S3A). Knockdown of ATF4 reduced the number of cells with CTPS filaments relative to controls under both glutamine/serum deprivation and EBSS + His conditions (Figure 3C). The protein levels of CTPS were similar in both the control and ATF4 knockdown groups, suggesting that assembly and disassembly of CTPS filaments was not affected by the level of CTPS (Figure S2B). These results show that expression of ATF4 is required for CTPS filament formation, suggesting that CTPS filaments may act as a regulator to integrate amino acid availability with nucleotide metabolism under conditions of nutritional restriction.

We investigated the molecular links between ATF4 and CTPS filament formation under starvation by performing transcriptional and metabolomics analysis to determine possible

mechanisms involved in CTPS filament formation. HEP-2 cells were cultured in DMEM or EBSS, with or without histidine, for 4 hr, and then total RNA was extracted for hybridization onto Affymetrix arrays (HTA2.0) (GEO: GSE105251). The expression of more than 600 genes for cells cultured in EBSS or EBSS + His was significantly different than those cultured in DMEM. However, there were no differences in gene expression between cells cultured in EBSS and those cultured in EBSS + His (Figures S4A–S4C). These data suggest that histidine treatment does not significantly alter gene expression but rather that nutritional deprivation in EBSS already triggers the transcriptional response. We used the Molecular Signature Database (MSigDB) to integrate the ATF4-targeted and histidine metabolism-related genes. We identified four genes among these two groups. Among them, MTHFD2, which is involved in mitochondrial one-carbon metabolism, was significantly upregulated (fold change > 2.0) in cells grown in EBSS/EBSS + His relative to those grown in DMEM (Figure 4A). Expression levels of MTHFD2 were confirmed by RT-qPCR and were consistent with those of the microarray data (Figures 4B, S4A, and S4B). The expression of the MTHFD2 transcript was significantly suppressed in ATF4

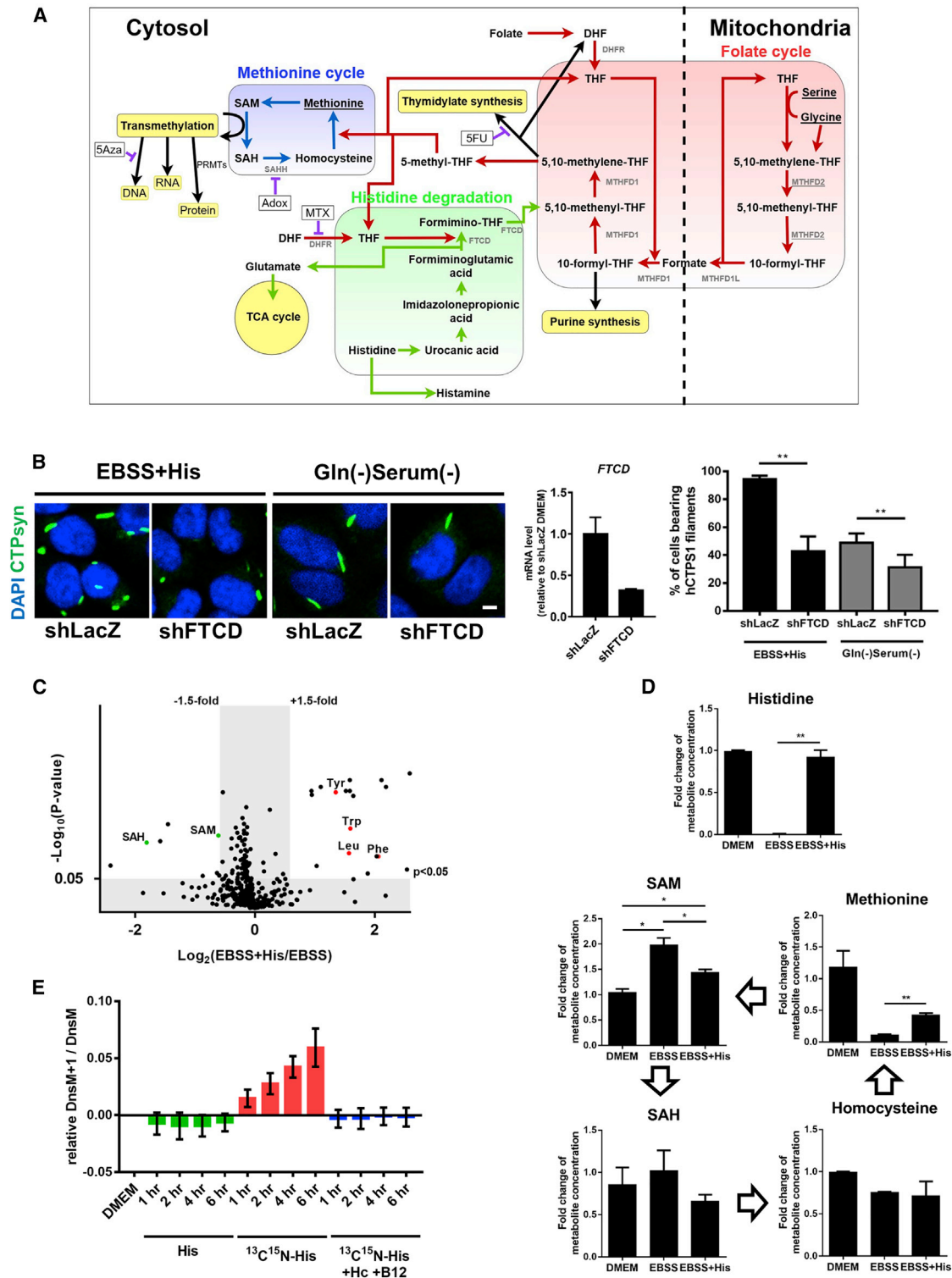


Figure 5. The Methionine Cycle Is Activated by Histidine

(A) Schematic diagram of one-carbon metabolism.

(B) The shLacZ and shFTCD stable knockdown HEP-2 cells were incubated in serum/Gln-negative medium or EBSS + His (50 μ M) for 24 hr, followed by immunostaining against CTPS (green) and DAPI (blue). The percentage of cells bearing CTPS filaments was calculated (mean \pm SD, $^{**}p < 0.01$). Scale bar: 10 μ m. FTCD mRNA expression was measured in shLacZ and shFTCD stable knockdown cells cultured in DMEM by qPCR.

(legend continued on next page)

knockdown cells under EBSS/EBSS + His and glutamine/serum deprivation conditions (Figure 4B). MTHFD2 knockdown also reduced filament formation (Figures 4C and 4D), suggesting that ATF4 may partly regulate CTPS filament formation by upregulating MTHFD2. MTHFD2 generates one-carbon units to produce formate for *de novo* purine and thymidylate synthesis and maintains the NADPH/NADP⁺ redox homeostasis (Ben-Sahra et al., 2016; Fan et al., 2014; Tedeschi et al., 2013; Vazquez et al., 2011). The addition of formate to MTHFD2 knockdown cells did not induce CTPS filament formation (Figure 4E), suggesting that one-carbon metabolism in mitochondria did not affect filament formation through formate-mediated *de novo* purine synthesis in the cytoplasm. However, treatment with the reactive oxygen species (ROS) hydrogen peroxide (H₂O₂) reduced the frequency of CTPS filament formation under glutamine/serum deprivation (Figure 4F), suggesting that a redox imbalance affects CTPS filament formation. Indeed, MTHFD2 knockdown under glutamine/serum deprivation condition, redox stress was increased (Figure 4G). Moreover, the reduction of NADH/NADPH in MTHFD2 knockdown may interfere the CTPS filament formation because NADH is required for *E. coli* CTPS filament formation (Habrian et al., 2016).

The Histidine-Dependent Cytosolic Folate Cycle and Methionine Cycle Are Essential for CTPS Filament Formation

There are two known pathways of histidine metabolism: histidine degradation and histamine synthesis (Figure 5A). Histidine can be degraded by deamination and hydrolysis and then converted to formiminoglutamic acid, which acts as the substrate of formimidoyltransferase cyclodeaminase (FTCD) to produce glutamate to fuel the TCA cycle and transfer one-carbon unit to the folate pool (Solans et al., 2000; Tabor et al., 1952). Histamine can only be synthesized from histidine by histidine decarboxylase, which is expressed mainly in mast cells and granulocytes and necessary for inflammation (Lazarus et al., 1986). We used the dihydrofolate reductase (DHFR) inhibitor methotrexate hydrate (MTX) to assess the effect of the folate cycle on filament formation. The frequency of CTPS filament formation was reduced in the presence of MTX (Figure S5A). However, the addition of histamine (100 μ M) or glutamate (200 μ M) to cells cultured in EBSS did not induce filament formation (Figure S5B). Indeed, knockdown of FTCD decreased the number of cells bearing CTPS filaments under glutamine/serum deprivation and EBSS + His conditions (Figures 5B and S5C). We then investigated how histidine influx triggers metabolic changes by analyzing the metabolomes of HEP-2 cells incubated in EBSS or EBSS + His for 4 hr. Principal-component analysis (PCA) showed moderate differences between the metabolomes of cells incubated in EBSS and EBSS + His, suggesting that meta-

bolic changes induced by histidine influx might induce CTPS filament formation (Figure S5D).

One-carbon metabolism is important for purine and thymidine synthesis, as well as methylation (Ducker and Rabinowitz, 2017). Thus, we examined the metabolite profiles to elucidate the importance of histidine-induced one-carbon metabolism. We found several significantly changed metabolites in the Metlin database (https://metlin.scripps.edu/landing_page.php?pgcontent=mainPage), on the basis of the volcano plots of the metabolomes of the EBSS and EBSS + His cultures. Notably, the levels of S-adenosylmethionine (SAM) and S-adenosylhomocysteine (SAH) in EBSS cultures were higher than those in EBSS + His cultures (Figure 5C). Methionine cycle metabolites were validated by mass spectrometry analysis via comparison with metabolite standards. The level of methionine was depleted in the EBSS cultures, but ~50% remained in the EBSS + His cultures relative to DMEM. Both SAM and SAH accumulated in cells cultured in EBSS relative to those in DMEM or EBSS + His, suggesting that transmethylation was blocked in EBSS and that histidine may release such blockage (Figure 5D). We used a stable isotope-labeling strategy using heavy histidine (¹³C¹⁵N-His) and found that histidine contributed 6% of methyl groups to methionine at 6 hr (Figures 5E and S5E). Increased labeling of methionine was blocked by adding homocysteine (Hc) and methylcobalamin (B₁₂). These data suggest that histidine contributes one carbon for methionine synthesis.

Protein Methylation Triggered by Histidine Is Required for Filament Formation

We assessed the role of methylation in the regulation of filament formation using the SAH hydrolase (SAHH) inhibitor Adox and the DNA methyltransferase (DNMT) inhibitor 5Aza, which inhibit global methylation and DNA methylation, respectively. Adox pre-treatment, followed by the addition of histidine, significantly reduced filament formation, whereas 5Aza treatment had little effect (Figure 6A). Consistently, filament formation was reduced by Adox treatment under glutamine/serum deprivation condition in HEP-2, HeLa, and U2OS cells (Figures 6B–6D, S6A, and S6B). PRMT5 is involved in metabolic regulation and the promotion of cell viability in response to starvation (Fay et al., 2014; Tsai et al., 2013). We tested whether PRMT5 is critical for filament formation in the presence of histidine under starvation by treating PRMT5 knockdown cells with histidine. Filament formation was significantly less in PRMT5 knockdown cells than controls (Figure 6E). Thus, protein methylation of CTPS might have a role in regulating filament formation, as post-translational modification has been previously suggested to regulate CTPS filament assembly (Pai et al., 2016). We investigated the role of protein methylation on CTPS filament formation by performing a monomeric

(C) Metabolomics profile of HEP-2 cells cultured in EBSS and EBSS + His. Log₂ fold change versus $-\log_{10}$ (p value).

(D) Normalized peak areas of methionine cycle and histidine metabolites from HEP-2 cells cultured in DMEM, EBSS, or EBSS + His for 4 hr detected by liquid chromatography (LC)/mass spectrometry (MS). Data were presented as the mean \pm SD of three independent experiments. *p < 0.05 and **p < 0.01.

(E) HEP-2 cells were incubated in DMEM and EBSS, with unlabeled histidine (200 μ M), ¹³C¹⁵N-histidine (200 μ M), or ¹³C¹⁵N-histidine plus homocysteine (Hc; 800 μ M) and methylcobalamin (B₁₂; 1 μ M) for indicated time points. The incorporation of ¹³C from labeled-histidine to methionine was expressed as "DnsM+1 / DnsM." The relative incorporation was calculated by subtracting the contribution of natural isotope distribution of unlabeled dansylated methionine (DnsM) (19.98% as measured from DMEM) from the signal of ¹³C-labeled DnsM. Data were presented as the mean \pm SD of three independent experiments.

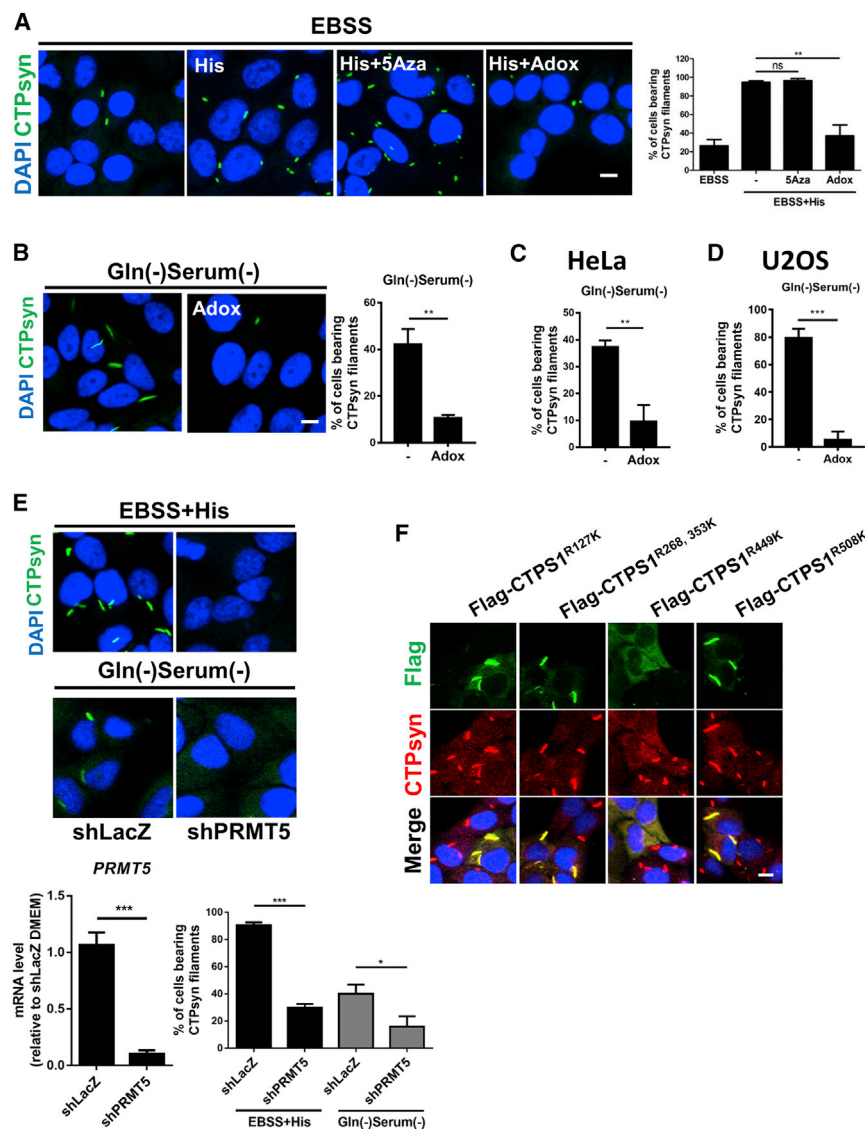


Figure 6. Protein Methylation Is Required for Filament Formation

(A) HEP-2 cells were cultured in the presence or absence of 5-Aza (20 μ M) and Adox (20 μ M) in EBSS for 24 hr and then treated with histidine for 24 hr. Control cells were grown in EBSS without histidine treatment. Cells were stained with anti-CTPS (green) and DAPI (blue). Scale bar: 10 μ m. (B) HEP-2 cells were cultured in serum/Gln-negative medium, with or without Adox (20 μ M) for 24 hr. (C and D) For 48 hr in HeLa (C) and U2OS (D) cells. (E) The shLacZ and shPRMT5 stable knockdown cells were treated with serum/Gln-negative medium or EBSS + His for 24 hr, followed by immunostaining against CTPS (green) and DAPI (blue). Scale bar: 10 μ m. PRMT5 mRNA expression was measured in shLacZ and shPRMT5 stable knockdown cells cultured in DMEM by qPCR. (F) HEP-2 cells overexpressing exogenous hCTPS1^{R127K}, hCTPS1^{R268,353K}, hCTPS1^{R449K}, or hCTPS1^{R508K} were incubated in EBSS + His for 24 hr, followed by immunostaining against Flag-CTPS (green), CTPS (red), and DAPI (blue). Scale bar: 10 μ m. Data are presented as mean \pm SD of three independent experiments. ns, not significant; * p < 0.05, ** p < 0.01 and *** p < 0.001.

peroxidase reporter (APEX2)-based proximal protein labeling assay in live cells (Hung et al., 2016; Lam et al., 2015). We used exogenous expression of hCTPS-APEX2 fusion proteins for *in vivo* labeling to enrich and isolate filamentous CTPS for mass spectrometry analysis. We identified five methylation candidate sites on arginine residues (Table S2) and constructed related mutants to assay filament formation in EBSS + His. Among the mutants, hCTPS1^{R449K} significantly affected filament formation in EBSS + His (Figure 6F), suggesting that methylation of the GAT domain is critical for CTPS filament assembly. Given that hCTPS1^{R449K} displayed similar enzymatic activity as hCTPS1^{WT}, this mutant should be able to form an active tetramer (Figures S6C and S6D). Altogether, our results demonstrate that protein methylation triggered by histidine is crucial for filament formation.

To understand the involvement of folate cycle coupled methyl cycle in histidine-induced CTPS filament formation, the role of purine and thymidine synthesis were evaluated. Inhibition of thy-

midylate synthase by 5-fluorouracil (5FU) did not affect histidine-induced filament formation (Figure S7A). ATP and guanosine triphosphate (GTP) levels were unchanged for up to 4 hr for both the EBSS and EBSS + His groups (Figure S7B). The formation of CTPS filaments was downregulated in the presence of the IMPDH inhibitor mycophenolic acid (MPA) (Figures S7C and S7D), suggesting that IMPDH2-mediated GTP synthesis may be required for CTPS filament formation. Serine and glycine are well known one-carbon unit contributors to folate

metabolism for *de novo* purine, thymidine synthesis, and re-methylation of Hc (Davis et al., 2004; Ducker et al., 2016; Mad-docks et al., 2016). CTPS filament formation was lower in the absence of histidine than that in its presence, under glutamine/serum deprivation (Figure 1C). The effect of serine and glycine on CTPS filament formation was similar to that observed in EBSS (Figure S7E). These results suggest that histidine catabolism coupled to folate metabolism specifically affects CTPS filament formation. Methionine treatment induced filament formation in 50% of the cells relative to histidine treatment (Figure S7E), confirming the important role of methylation in filament formation.

We investigated the role of folate-mediated metabolic pathways in cancers by analyzing the metabolic pathways involved in this study using RNA sequencing (RNA-seq) datasets of various cancer types from The Cancer Genome Atlas (TCGA) database. The expression difference between normal and tumor

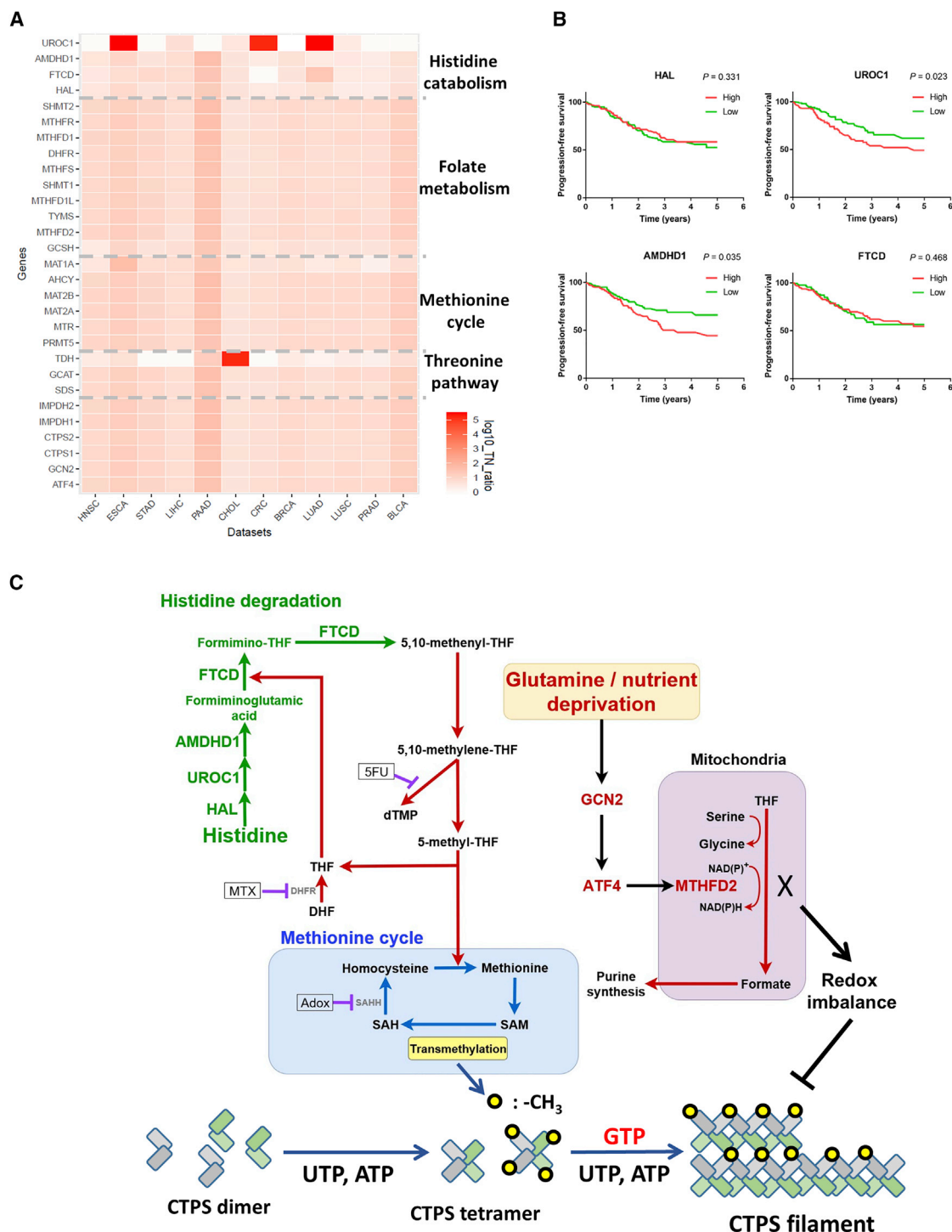


Figure 7. Histidine Catabolism Is Associated with Cancer Progression

(A) The differential expression of genes that are involved in histidine catabolism, folate metabolism, methionine cycle, and threonine pathway is analyzed using RNA-seq datasets from The Cancer Genome Atlas (TCGA) database. The differentially expressed levels of each gene in tumor and normal tissue are presented in the color bar. The white color indicates no significant difference. HNSC, head-neck squamous cell carcinoma; ESCA, esophageal carcinoma; STAD, stomach adenocarcinoma; CRC, colorectal carcinoma; BRCA, breast cancer; LIHC, liver hepatocellular carcinoma; PAAD, pancreatic adenocarcinoma; CHOL, cholangiocarcinoma; LUAD, lung adenocarcinoma; LUSC, lung squamous cell carcinoma; PRAD, prostate adenocarcinoma; BLCA, bladder carcinoma.

(legend continued on next page)

tissues of the key genes in these metabolic pathways are illustrated in [Figure 7A](#). These data revealed that the histidine catabolism pathway (UROC1) is activated in several cancer types, suggesting that histidine may be the major fuel source for methylation in some cancer cells. We evaluated the potential role of the histidine degradation pathway in patients with colorectal carcinoma (CRC). The two genes UROC1 and AMDHD1 were associated with recurrence in progression-free survival analysis. Patients who exhibited higher expression of UROC1 and AMDHD1 had poor outcomes in Kaplan-Meier curve analysis ([Figure 7B](#)). Overall, these results highlight the physiological role of histidine in tumor metabolism.

DISCUSSION

Membraneless organelles allow rapid phase transition through the assembly and disassembly of macromolecules in response to environmental cues. Here we showed that cells uptake histidine to trigger filament formation during glutamine deprivation. We demonstrated that histidine donates one carbon to the methionine cycle through cytosolic folate cycle, which is required for CTPS filament assembly during glutamine deficiency and nutrient deprivation ([Figure 7C](#)). Furthermore, we revealed a correlation between histidine catabolism and patient survival in colorectal cancer analyzed in TCGA database.

Methylation inhibitors, methyltransferase protein knockdown, and point mutations of potential CTPS methylation sites all demonstrated that protein methylation is required for CTPS filament formation. Histone hypermethylation is observed in the tumor core region because of decreased glutamine levels and results in cancer cell dedifferentiation, suggesting the critical role of transmethylation during glutamine deprivation ([Pan et al., 2016](#)). However, methionine displayed only half the capacity of histidine to induce filament formation ([Figure S7E](#)). It is known that the transmethylation reaction in the methionine cycle requires the cytosolic folate cycle to re-methylate Hc, as the accumulation of SAH, a precursor of Hc in the cycle, would block methyltransferase activity ([Ussdin et al., 1979](#)). Therefore, methionine could partially, but not fully, promote transmethylation activity. In addition, depletion of methionine from the EAA pool had only a minor effect on filament formation. Consistent with these results, in the absence of histidine, CTPS filaments could not form under conditions of glutamine/serum deprivation, even while serine, glycine, and methionine were presented. Collectively, the amino acid balance is critical for CTPS filament formation under physiological conditions that mimic the interior of tumors.

Aside from histidine, serine and glycine also serve as inputs of one-carbon metabolism, and serine was recently shown to participate in the methionine cycle by producing SAM ([Maddocks et al., 2016](#)). Our results showed that neither serine nor glycine significantly induced filament formation ([Figure S7E](#)), implying that serine- and glycine-mediated folate metabolism

may not contribute to the methylation events that are required for CTPS filament formation. Additionally, in the context of glutamine/serum deprivation, the influx of amino acids, such as histidine, methionine, and serine, was increased ([Figure 3A](#)), suggesting that folate metabolism coupled to the methylation cycle may be an adaptive strategy for cellular homeostasis in cancer cells under nutrient starvation.

Our observations of a tetrameric conformation and glutamine-induced disassembly of CTPS filament are consistent with those of previous studies ([Calise et al., 2014](#); [Gou et al., 2014](#); [Lynch et al., 2017](#)). Here, we also demonstrated that UTP binding and linker region interactions are critical for filament formation ([Figures 2A and S2A](#)). We propose that UTP- rather than CTP-mediated CTPS filament formation may function in a “semi-active” manner, as UTP was preserved in the filament structure along with CTPS ([Figure S2A](#)). Once glutamine levels return to normal, filamentous CTPS disassembles and immediately reactivates, contributing to a rapid recovery from the quiescent status ([Figure S2E](#)). Indeed, previous studies of *Drosophila* CTPS suggest that the filamentous structure is required for optimal enzymatic activity ([Wang et al., 2015](#)). Here, we also showed that protein methylation is required for polymerization of CTPS tetramers ([Figure 6](#)). The size of filaments revealed by immunostaining is much larger than the single filaments observed in the cryo-EM structure study, suggesting that CTPS filaments in cells may form through bundling of individual filaments ([Liu, 2011](#); [Lynch et al., 2017](#)). We suspect that methylation may facilitate the bundling of filaments or their interaction with associated proteins required for polymerization *in vivo*.

We found that CTPS is preserved by forming filaments, which is a strategy for maintaining homeostasis during starvation ([Figure 2E](#)). Furthermore, preserved CTPS provided growth advantages after nutrient replenishment ([Figure S2F](#)). Decreased glutamine levels have been observed in the tumor core region ([Pan et al., 2016](#)). It may be informative to examine the spatial distribution of CTPS filaments in cancer tissues. Although cancer cells exhibit a quiescent state under glutamine deprivation, filament assembly might act as a reservoir for the preservation of proteins under adverse environmental conditions. It may be informative to further analyze the role of histidine in CTPS-related cancer. This would shed light on a fundamental issue in cancer biology, explaining how cancer cells cope with nutrient restriction and become highly dependent on *de novo* nucleotide synthesis for cell growth. This finding may provide directions for cancer therapy.

STAR★METHODS

Detailed methods are provided in the online version of this paper and include the following:

- [KEY RESOURCES TABLE](#)
- [CONTACT FOR REAGENT AND RESOURCE SHARING](#)

(B) Progression-free survival analysis for CRC patients (n = 242) with four genes (*HAL*, *UROC1*, *AMDHD1*, and *FTCD*) involving histidine catabolism. The patients were divided into two groups (n = 121 for each group) according to the median expression of these genes. The high expression of genes were identified as “red” and low expression of genes as “green.”

(C) Model: the molecular mechanisms of CTPS filament formation during nutrient deprivation. Histidine-mediated one-carbon metabolism coupled methionine cycle act cooperatively with the upregulation of mitochondrial MTHFD2 to promote bundling of CTPS filament.

● EXPERIMENTAL MODEL AND SUBJECT DETAILS

● METHOD DETAILS

- Cell culture
- Immunofluorescent staining
- Plasmid construction
- Western blotting
- Cell growth and bromodeoxyuridine (BrdU) incorporation assays
- Recombinant lentivirus shRNA gene knockdown
- Gene expression
- Intracellular ROS measurement
- Protein structure modeling
- Measurement of intracellular amino acids
- Detection of CTPS1 methylation sites
- Untargeted metabolite analysis
- Targeted metabolite analysis
- Dansylation labeling and LC-MS analysis
- Measurement of labeling UTP and CTP
- Progression-free survival analysis

● QUANTIFICATION AND STATISTICAL ANALYSIS

● DATA AND SOFTWARE AVAILABILITY

- Microarray analysis

SUPPLEMENTAL INFORMATION

Supplemental Information includes seven figures and two tables and can be found with this article online at <https://doi.org/10.1016/j.celrep.2018.08.007>.

ACKNOWLEDGMENTS

We thank the Genomic Medicine Core Laboratory of Chang Gung Memorial Hospital, Metabolomics Core Laboratory, Proteomics Core Laboratory, Microscopy Center, and Bioinformatics Core Laboratory of Chang Gung University for assistance with microarray analysis, untargeted and targeted metabolomics analysis, proteomic analysis, image capture, and TCGA database analysis, respectively. We thank the National RNAi Core Facility at Academia Sinica for providing short hairpin RNA (shRNA) reagents and related services. We thank Widelitz Randall, Juli Wu, Zee-Fen Chang, and Laura Nilson for their comments on the manuscript. This work was funded by the Ministry of Science and Technology, Taiwan (MOST 103-2311-B-182-004-MY3 to L.-M.P. and MOST 106-2811-B-182-002 to P.-Y.W.); the Chang Gung Memorial Hospital, Taiwan (CMRPD1E0271-3 to L.-M.P. and Biosignature Research Grant CIRPD3B0013); the Ministry of Education (MOE), Taiwan (EMRPD1G0041 to L.-M.P.); and the Molecular Medicine Research Center, Chang Gung University, from The Featured Areas Research Center Program within the framework of the Higher Education Sprout Project by the MOE in Taiwan.

AUTHOR CONTRIBUTIONS

W.-C.L. and L.-M.P. designed the study and wrote the manuscript. W.-C.L., A.C., P.-Y.W., and Y.-H.L. performed the experiments. C.-C.C. confirmed the effect of histidine on filament formation. S.-C.H. performed immunofluorescence staining. H.-Y.T., M.-L.C., M.-S.S., Y.-J.H., Y.-T.C., and K.-Y.C. conducted metabolomics analysis. Y.-T.L. and J.-S.Y. conducted proteomics analysis. C.-S.T., J.-D.L., T.-W.C., and Y.-S.C. conducted bioinformatics analysis. C.-T.Y., T.-Y.L., J.-L.L., and L.-Y.S. provided reagents and conceptual advice.

DECLARATION OF INTERESTS

The authors declare no competing interests.

Received: November 3, 2017

Revised: May 11, 2018

Accepted: August 3, 2018

Published: September 4, 2018

REFERENCES

- An, S., Kumar, R., Sheets, E.D., and Benkovic, S.J. (2008). Reversible compartmentalization of de novo purine biosynthetic complexes in living cells. *Science* 320, 103–106.
- Aughey, G.N., Grice, S.J., and Liu, J.L. (2016). The interplay between Myc and CTP synthase in *Drosophila*. *PLoS Genet.* 12, e1005867.
- Barry, R.M., Bitbol, A.F., Lorestani, A., Charles, E.J., Habrian, C.H., Hansen, J.M., Li, H.J., Baldwin, E.P., Wingreen, N.S., Kollman, J.M., and Gitai, Z. (2014). Large-scale filament formation inhibits the activity of CTP synthetase. *eLife* 3, e03638.
- Ben-Sahra, I., Hoxhaj, G., Ricoult, S.J.H., Asara, J.M., and Manning, B.D. (2016). mTORC1 induces purine synthesis through control of the mitochondrial tetrahydrofolate cycle. *Science* 351, 728–733.
- Brangwynne, C.P., Eckmann, C.R., Courson, D.S., Rybarska, A., Hoege, C., Gharakhani, J., Jülicher, F., and Hyman, A.A. (2009). Germline P granules are liquid droplets that localize by controlled dissolution/condensation. *Science* 324, 1729–1732.
- Calise, S.J., Carcamo, W.C., Krueger, C., Yin, J.D., Purich, D.L., and Chan, E.K. (2014). Glutamine deprivation initiates reversible assembly of mammalian rods and rings. *Cell. Mol. Life Sci.* 71, 2963–2973.
- Carcamo, W.C., Satoh, M., Kasahara, H., Terada, N., Hamazaki, T., Chan, J.Y., Yao, B., Tamayo, S., Covini, G., von Mühlen, C.A., and Chan, E.K. (2011). Induction of cytoplasmic rods and rings structures by inhibition of the CTP and GTP synthetic pathway in mammalian cells. *PLoS ONE* 6, e29690.
- Chen, K., Zhang, J., Tastan, O.Y., Deussen, Z.A., Siswick, M.Y., and Liu, J.L. (2011). Glutamine analogs promote cytoophidium assembly in human and *Drosophila* cells. *J. Genet. Genomics* 38, 391–402.
- Chen, R., Zou, Y., Mao, D., Sun, D., Gao, G., Shi, J., Liu, X., Zhu, C., Yang, M., Ye, W., et al. (2014). The general amino acid control pathway regulates mTOR and autophagy during serum/glutamine starvation. *J. Cell Biol.* 206, 173–182.
- Chou, H.Y., Lin, Y.H., Shiu, G.L., Tang, H.Y., Cheng, M.L., Shiao, M.S., and Pai, L.M. (2014). ADI1, a methionine salvage pathway enzyme, is required for *Drosophila* fecundity. *J. Biomed. Sci.* 21, 64.
- Davis, S.R., Stacpoole, P.W., Williamson, J., Kick, L.S., Quinlivan, E.P., Coats, B.S., Shane, B., Bailey, L.B., and Gregory, J.F., 3rd. (2004). Tracer-derived total and folate-dependent homocysteine remethylation and synthesis rates in humans indicate that serine is the main one-carbon donor. *Am. J. Physiol. Endocrinol. Metab.* 286, E272–E279.
- Ducker, G.S., and Rabinowitz, J.D. (2017). One-carbon metabolism in health and disease. *Cell Metab.* 25, 27–42.
- Ducker, G.S., Chen, L., Morscher, R.J., Ghergurovich, J.M., Esposito, M., Teng, X., Kang, Y., and Rabinowitz, J.D. (2016). Reversal of cytosolic one-carbon flux compensates for loss of the mitochondrial folate pathway. *Cell Metab.* 24, 640–641.
- Fan, J., Ye, J., Kamphorst, J.J., Shlomi, T., Thompson, C.B., and Rabinowitz, J.D. (2014). Quantitative flux analysis reveals folate-dependent NADPH production. *Nature* 510, 298–302.
- Fay, M.M., Clegg, J.M., Uchida, K.A., Powers, M.A., and Ullman, K.S. (2014). Enhanced arginine methylation of programmed cell death 4 protein during nutrient deprivation promotes tumor cell viability. *J. Biol. Chem.* 289, 17541–17552.
- Gou, K.M., Chang, C.C., Shen, Q.J., Sung, L.Y., and Liu, J.L. (2014). CTP synthase forms cytoophidia in the cytoplasm and nucleus. *Exp. Cell Res.* 323, 242–253.
- Guo, K., and Li, L. (2009). Differential ¹²C/¹³C-isotope dansylation labeling and fast liquid chromatography/mass spectrometry for absolute and relative quantification of the metabolome. *Anal. Chem.* 81, 3919–3932.

- Habrian, C., Chandrasekhara, A., Shahrivini, B., Hua, B., Lee, J., Jesinghaus, R., Barry, R., Gitai, Z., Kollman, J., and Baldwin, E.P. (2016). Inhibition of *Escherichia coli* CTP Synthetase by NADH and Other Nicotinamides and Their Mutual Interactions with CTP and GTP. *Biochemistry* 55, 5554–5565.
- Harding, H.P., Zhang, Y., Zeng, H., Novoa, I., Lu, P.D., Calfon, M., Sadri, N., Yun, C., Popko, B., Paules, R., et al. (2003). An integrated stress response regulates amino acid metabolism and resistance to oxidative stress. *Mol. Cell* 11, 619–633.
- Hung, V., Udeshi, N.D., Lam, S.S., Loh, K.H., Cox, K.J., Pedram, K., Carr, S.A., and Ting, A.Y. (2016). Spatially resolved proteomic mapping in living cells with the engineered peroxidase APEX2. *Nat. Protoc.* 11, 456–475.
- Hyman, A.A., Weber, C.A., and Jülicher, F. (2014). Liquid-liquid phase separation in biology. *Annu. Rev. Cell Dev. Biol.* 30, 39–58.
- Ingerson-Mahar, M., Briegel, A., Werner, J.N., Jensen, G.J., and Gitai, Z. (2010). The metabolic enzyme CTP synthase forms cytoskeletal filaments. *Nat. Cell Biol.* 12, 739–746.
- Kedersha, N.L., Gupta, M., Li, W., Miller, I., and Anderson, P. (1999). RNA-binding proteins TIA-1 and TIAR link the phosphorylation of eIF-2 alpha to the assembly of mammalian stress granules. *J. Cell Biol.* 147, 1431–1442.
- Kilberg, M.S., Shan, J., and Su, N. (2009). ATF4-dependent transcription mediates signaling of amino acid limitation. *Trends Endocrinol. Metab.* 20, 436–443.
- Kim, C.S., Cho, S.H., Chun, H.S., Lee, S.Y., Endou, H., Kanai, Y., and Kim, D.K. (2008). BCH, an inhibitor of system L amino acid transporters, induces apoptosis in cancer cells. *Biol. Pharm. Bull.* 31, 1096–1100.
- Kizaki, H., Williams, J.C., Morris, H.P., and Weber, G. (1980). Increased cytidine 5'-triphosphate synthetase activity in rat and human tumors. *Cancer Res.* 40, 3921–3927.
- Klawitter, J., Schmitz, V., Klawitter, J., Leibfritz, D., and Christians, U. (2007). Development and validation of an assay for the quantification of 11 nucleotides using LC/LC-electrospray ionization-MS. *Anal. Biochem.* 365, 230–239.
- Lam, S.S., Martell, J.D., and Kamer, K.J. (2015). Directed evolution of APEX2 for electron microscopy and proximity labeling. *Nat. Methods* 12, 51–54.
- Lazarus, S.C., McCabe, L.J., Nadel, J.A., Gold, W.M., and Leikauf, G.D. (1986). Effects of mast cell-derived mediators on epithelial cells in canine trachea. *Am. J. Physiol.* 251, C387–C394.
- Liu, J.L. (2010). Intracellular compartmentation of CTP synthase in *Drosophila*. *J. Genet. Genomics* 37, 281–296.
- Liu, J.L. (2011). The enigmatic cytoophidium: compartmentation of CTP synthase via filament formation. *BioEssays* 33, 159–164.
- Lynch, E.M., Hicks, D.R., Shepherd, M., Endrizzi, J.A., Maker, A., Hansen, J.M., Barry, R.M., Gitai, Z., Baldwin, E.P., and Kollman, J.M. (2017). Human CTP synthase filament structure reveals the active enzyme conformation. *Nat. Struct. Mol. Biol.* 24, 507–514.
- Maddocks, O.D., Labuschagne, C.F., Adams, P.D., and Vousden, K.H. (2016). Serine metabolism supports the methionine cycle and DNA/RNA methylation through de novo ATP synthesis in cancer cells. *Mol. Cell* 61, 210–221.
- McCluskey, G.D., Mohamady, S., Taylor, S.D., and Bearne, S.L. (2016). Exploring the potent inhibition of CTP synthase by gemcitabine-5'-triphosphate. *ChemBioChem* 17, 2240–2249.
- Munger, J., Bajad, S.U., Collier, H.A., Shenk, T., and Rabinowitz, J.D. (2006). Dynamics of the cellular metabolome during human cytomegalovirus infection. *PLoS Pathog.* 2, e132.
- Noree, C., Sato, B.K., Broyer, R.M., and Wilhelm, J.E. (2010). Identification of novel filament-forming proteins in *Saccharomyces cerevisiae* and *Drosophila melanogaster*. *J. Cell Biol.* 190, 541–551.
- Noree, C., Monfort, E., Shiao, A.K., and Wilhelm, J.E. (2014). Common regulatory control of CTP synthase enzyme activity and filament formation. *Mol. Biol. Cell* 25, 2282–2290.
- O'Connell, J.D., Zhao, A., Ellington, A.D., and Marcotte, E.M. (2012). Dynamic reorganization of metabolic enzymes into intracellular bodies. *Annu. Rev. Cell Dev. Biol.* 28, 89–111.
- Pai, L.M., Wang, P.Y., Lin, W.C., Chakraborty, A., Yeh, C.T., and Lin, Y.H. (2016). Ubiquitination and filamentous structure of cytidine triphosphate synthase. *Fly (Austin)* 10, 108–114.
- Pan, M., Reid, M.A., Lowman, X.H., Kulkarni, R.P., Tran, T.Q., Liu, X., Yang, Y., Hernandez-Davies, J.E., Rosales, K.K., Li, H., et al. (2016). Regional glutamine deficiency in tumours promotes dedifferentiation through inhibition of histone demethylation. *Nat. Cell Biol.* 18, 1090–1101.
- Pappa-Louisi, A., Nikitas, P., Agrafiotou, P., and Papageorgiou, A. (2007). Optimization of separation and detection of 6-aminoquinolyl derivatives of amino acids by using reversed-phase liquid chromatography with on line UV, fluorescence and electrochemical detection. *Anal. Chim. Acta* 593, 92–97.
- Petersen, E.F., Goddard, T.D., Huang, C.C., Couch, G.S., Greenblatt, D.M., Meng, E.C., and Ferrin, T.E. (2004). UCSF Chimera—a visualization system for exploratory research and analysis. *J. Comput. Chem.* 25, 1605–1612.
- Solans, A., Estivill, X., and de la Luna, S. (2000). Cloning and characterization of human FTCD on 21q22.3, a candidate gene for glutamate formiminotransferase deficiency. *Cytogenet. Cell Genet.* 88, 43–49.
- Strochlic, T.I., Stavrides, K.P., Thomas, S.V., Nicolas, E., O'Reilly, A.M., and Peterson, J.R. (2014). Ack kinase regulates CTP synthase filaments during *Drosophila* oogenesis. *EMBO Rep.* 15, 1184–1191.
- Tabor, H., Mehler, A.H., Hayaishi, O., and White, J. (1952). Urocanic acid as an intermediate in the enzymatic conversion of histidine to glutamic and formic acids. *J. Biol. Chem.* 196, 121–128.
- Tedeschi, P.M., Markert, E.K., Gounder, M., Lin, H., Dvorzhinski, D., Dolfi, S.C., Chan, L.L., Qiu, J., DiPaola, R.S., Hirshfield, K.M., et al. (2013). Contribution of serine, folate and glycine metabolism to the ATP, NADPH and purine requirements of cancer cells. *Cell Death Dis.* 4, e877.
- Tsai, W.W., Niessen, S., Goebel, N., Yates, J.R., 3rd, Guccione, E., and Montminy, M. (2013). PRMT5 modulates the metabolic response to fasting signals. *Proc. Natl. Acad. Sci. U S A* 110, 8870–8875.
- Usdin, E., Borchardt, R.T., and Creveling, C.R. (1979). Transmethylation: Proceedings of the Conference on Transmethylation, Bethesda, Maryland, U.S.A., on October 16–19, 1978 (New York: Elsevier-North Holland).
- van den Berg, A.A., van Lenthe, H., Busch, S., de Korte, D., Roos, D., van Kullenburg, A.B., and van Gennip, A.H. (1993). Evidence for transformation-related increase in CTP synthetase activity in situ in human lymphoblastic leukemia. *Eur. J. Biochem.* 216, 161–167.
- Vazquez, A., Markert, E.K., and Oltvai, Z.N. (2011). Serine biosynthesis with one carbon catabolism and the glycine cleavage system represents a novel pathway for ATP generation. *PLoS ONE* 6, e25881.
- Wang, P.Y., Lin, W.C., Tsai, Y.C., Cheng, M.L., Lin, Y.H., Tseng, S.H., Chakraborty, A., and Pai, L.M. (2015). Regulation of CTP synthase filament formation during DNA endoreplication in *Drosophila*. *Genetics* 201, 1511–1523.
- Williams, J.C., Kizaki, H., Weber, G., and Morris, H.P. (1978). Increased CTP synthetase activity in cancer cells. *Nature* 271, 71–73.

STAR★METHODS

KEY RESOURCES TABLE

REAGENT or RESOURCE	SOURCE	IDENTIFIER
Antibodies		
ATF4	Proteintech Group	Cat# 10835-1-AP RRID:AB_2058600
MTHFD2	Proteintech Group	Cat# 12270-1-AP; RRID: AB_2147525
GCN2	Cell Signaling Technology	Cat# 3302 RRID:AB_2277617
Flag	Sigma-Aldrich	Cat# F1804 RRID:AB_262044
CTP synthase (Western blots)	GeneTex	Cat# GTX115010 RRID:AB_10621165
CTP synthase (immunostaining for cell lines)	Santa Cruz Biotechnology	Cat# sc-134457 RRID:AB_2008726
BrdU	Becton Dickinson and Company	Cat# 555627 RRID:AB_10015222
Actin	Millipore	Cat# MAB1501 RRID:AB_2223041
Bacterial and Virus Strains		
HIT-DH5a	RBC HIT Competent Cell	Cat# RH617-J80
Chemicals, Peptides, and Recombinant Proteins		
polybrene	Sigma-Aldrich	Cat# 107689
puromycin	Invivogen	Cat# ant-pr-1
Protease inhibitor	Roche	Cat# 11697498001
bromodeoxyuridine (BrdU)	Sigma-Aldrich	Cat# 10280879001
Adenosine-2',3'-dialdehyde (Adox)	Sigma-Aldrich	Cat#A7154
Decitabine (5-Aza-2'-deoxycytidine)	Sigma-Aldrich	Cat#A3656
Methotrexate hydrate (MTX)	Sigma-Aldrich	Cat#M8407
Histamine dihydrochloride	Sigma-Aldrich	Cat#53300
2-Amino-2-norbornanecarboxylic acid (BCH)	Sigma-Aldrich	Cat#A7902
Cycloheximide	Sigma-Aldrich	Cat#C7698
5-Fluorouracil (5FU)	Sigma-Aldrich	Cat#F6627
dichlorohydrofluorescein diacetate	Invitrogen	Cat#D399
L-HISTIDINE:HCL:H2O (< 5% D) (13C6, 97-99%; 15N3, 97-99%)	Cambridge Isotope Laboratories	Cat#CNLM-758-PK
URIDINE (13C9, 98%; 15N2, 96-98%)	Cambridge Isotope Laboratories	Cat# CNLM-3809-PK
MEM Amino Acids Solution, 50X	Gibco	Cat#11130051
Glutamine	GIBCO	Cat#25030081
Arginine	Sigma-Aldrich	Cat#A5131
Cysteine	Sigma-Aldrich	Cat#C7352
Glutamate	Sigma-Aldrich	Cat#G8415
Histidine	Sigma-Aldrich	Cat#H5659
Isoleucine	Sigma-Aldrich	Cat#I2752
Leucine	Sigma-Aldrich	Cat#L8912
Lysine	Sigma-Aldrich	Cat#L8662
Methionine	Sigma-Aldrich	Cat#M9625
Phenylalanine	Sigma-Aldrich	Cat#P5482
Threonine	Sigma-Aldrich	Cat#T8625
Tryptophan	Sigma-Aldrich	Cat#T0254
Tyrosine	Sigma-Aldrich	Cat#T8566
Valine	Sigma-Aldrich	Cat#V0500

(Continued on next page)

Continued

REAGENT or RESOURCE	SOURCE	IDENTIFIER
Deposited Data		
Raw data of microarray	This paper	GEO: GSE105251
Experimental Models: Cell Lines		
HEp2	ATCC	CCL-23
HeLa	ATCC	CCL2
U2OS	ATCC	HTB-96
HEK293T	ATCC	CRL-11268
Oligonucleotides		
RT-qPCR primer ATF4_F: ATGACCGAAATGAGCTTCCTG	This paper	N/A
RT-qPCR primer ATF4_R: GCTGGAGAACCCATGAGGT	This paper	N/A
RT-qPCR primer MTHFD2_F: CTGCGACTTCTCTAATGTCTGCG	This paper	N/A
RT-qPCR primer MTHFD2_R: CTCGCCAACCAGGATCACACA	This paper	N/A
RT-qPCR primer PRMT5_F: GCCATCCCAACCGAGA	This paper	N/A
RT-qPCR primer PRMT5_R: CGCCAGAAACGCACA	This paper	N/A
RT-qPCR primer FTCD_F: CCAATCTTCTGGACTTTGAGGTCAC	This paper	N/A
RT-qPCR primer FTCD_R: AAGAGGTTCTCCTTCTCGCAGTA	This paper	N/A
Cloning primer hCTPS1_F: TAAGCATCTAGAATGAAGTACATTC TGGTTACTGGTGG	This paper	N/A
Cloning primer hCTPS1_R: ATTGCTGGATCCTCAGTCATGATT TATTGATGGAACTTC	This paper	N/A
Site directed mutagenesis primer hCTPS1 ^{R127K} _F: TGCAATCCA GGAGTGGGTGATGAAACAGGCGTTAAT	This paper	N/A
Site directed mutagenesis primer hCTPS1 ^{R127K} _R: ATTAACGCC TGTTCATCACCCACTCCTGGATTGCA	This paper	N/A
Site directed mutagenesis primer hCTPS1 ^{G148A} _F: GTGTTATTG AGCTTGCTGGAACCGTGGGGGA	This paper	N/A
Site directed mutagenesis primer hCTPS1 ^{G148A} _R: TCCCCCAC GGTCCAGCAAGCTCAATAACAC	This paper	N/A
Site directed mutagenesis primer hCTPS1 ^{E161K} _F: ACATAGAAA GCATGCCCTTTATTAAGGCCTTCCGTC	This paper	N/A
Site directed mutagenesis primer hCTPS1 ^{E161K} _R: GACGGAAG GCCTTAATAAAGGCATGCTTTCTATGT	This paper	N/A
Site directed mutagenesis primer hCTPS1 ^{R268K} _F: GGAGCAAG GGGTTGTAGATTATTTCTTAAAGACTTGACCTTCC	This paper	N/A
Site directed mutagenesis primer hCTPS1 ^{R268K} _R: GGAAGGTC AAGTCTTTAAGAAAATAATCTACAACCCCTTGCTCC	This paper	N/A
Site directed mutagenesis primer hCTPS1 ^{R294D} _F: GATGGCTG ACAGATATGATGACTTGCTGGAGACCTGCTC	This paper	N/A
Site directed mutagenesis primer hCTPS1 ^{R294D} _R: GAGCAGGT CTCCAGCAAGTCATCATATCTGTCAGCCATC	This paper	N/A
Site directed mutagenesis primer hCTPS1 ^{R353K} _F: CGCAAGAA GAGCCCGTGAGTACCACGAAGCTTGGCA	This paper	N/A
Site directed mutagenesis primer hCTPS1 ^{R353K} _R: TGCCAAGC TTCGTGGTACTTCACGGGCTCTTCTTGCG	This paper	N/A
Site directed mutagenesis primer hCTPS1 ^{R449K} _F: CAGATGGG CGGAACCATGAAGCTGGGCAAG	This paper	N/A
Site directed mutagenesis primer hCTPS1 ^{R449K} _R: CTTGCCCA GCTTCATGGTTCGCCCATCTG	This paper	N/A
Site directed mutagenesis primer hCTPS1 ^{R508K} _F: CCAAGATGT TGAAGGAGAGAAAATGGAAATTGTGGAGTTAG	This paper	N/A
Site directed mutagenesis primer hCTPS1 ^{R508K} _R: CTAATCC ACAATTCCATTTCTCCTTCAACATCTTGG	This paper	N/A

(Continued on next page)

Continued

REAGENT or RESOURCE	SOURCE	IDENTIFIER
Recombinant DNA		
p3xflag-myc-cmv-26	Sigma-Aldrich	E7283
p3xflag-hCTPS1 ^{WT} -cmv-26	This paper	N/A
p3xflag-hCTPS1 ^{R127K} -cmv-26	This paper	N/A
p3xflag-hCTPS1 ^{G148A} -cmv-26	This paper	N/A
p3xflag-hCTPS1 ^{E161K} -cmv-26	This paper	N/A
p3xflag-hCTPS1 ^{R268K} -cmv-26	This paper	N/A
p3xflag-hCTPS1 ^{R294D} -cmv-26	This paper	N/A
p3xflag-hCTPS1 ^{R353K} -cmv-26	This paper	N/A
p3xflag-hCTPS1 ^{R449K} -cmv-26	This paper	N/A
p3xflag-hCTPS1 ^{R508K} -cmv-26	This paper	N/A
shRNA targeting sequence: LacZ	NRC	Clone ID: TRCN0000072224
shRNA targeting sequence: EIF2AK4 (GCN2)	NRC	Clone ID: TRCN0000300850
shRNA targeting sequence: ATF4	NRC	Clone ID: TRCN0000013573
shRNA targeting sequence: MTHFD2	NRC	Clone ID: TRCN0000036551
shRNA targeting sequence: PRMT5	NRC	Clone ID: TRCN0000107086
shRNA targeting sequence: FTCD	NRC	Clone ID: TRCN0000035000
Software and Algorithms		
Prism 6	Graphpad	N/A
VisionWorks Analysis Software	UVP	N/A
QuickChange site-directed mutagenesis	Agilent	N/A

CONTACT FOR REAGENT AND RESOURCE SHARING

Further information and requests for resources and reagents should be directed to and will be fulfilled by the Lead Contact, Li-Mei Pai (pai@mail.cgu.edu.tw).

EXPERIMENTAL MODEL AND SUBJECT DETAILS

The HEP2 cell line is derived from human epidermoid carcinoma of the larynx, the HeLa cell line is derived from human cervical adenocarcinoma tissue, the U2OS cell line is derived from human osteosarcoma and the HEK293T cells are derived from human embryonic kidney tissue. All cells were maintained in DMEM supplemented with 10% fetal bovine serum and 1x Anti-Anti at 37°C in a humidified incubator under 5% CO₂.

METHOD DETAILS

Cell culture

Human HEP-2, HeLa, U2OS and HEK293 T cells were cultured in Dulbecco's Modified Eagle's Medium (GIBCO) supplemented with 10% fetal bovine serum and 1 × antibiotic antimycotic (GIBCO). Cells were maintained at 37°C under 5% CO₂.

Immunofluorescent staining

5 × 10⁴ human HEP-2 cells were seeded onto glass coverslips in 24-well plates and incubated overnight. Culture medium was replaced with conditional medium (serum negative DMEM, glutamine negative DMEM, serum/glutamine negative DMEM, EBSS, EBSS + essential AA and EBSS + His) for 24 h. Cells were washed with PBS once and fixed in 4% formaldehyde for 10 min, followed by two rinses in PBS. Cells were further fixed in 100% methanol (−20°C) for 2 min, washed twice in PBS, and blocked and permeabilized with blocking buffer (2% BSA and 0.2% Triton X-100 in PBS) for 20 min. Cells were incubated with primary antibody in dilution buffer (2% BSA in PBS) overnight at 4°C, washed 3 times in PBST (0.05% Tween 20 in PBS), and incubated with secondary antibody in dilution buffer (2% BSA in PBS) for 1 h. Coverslips were mounted in mounting medium and samples examined by confocal microscopy (Zeiss LSM 510 Meta confocal microscope).

Plasmid construction

Human CTPS PCR cloning fragments were amplified from extracted RNA of HEP-2 cells and cloned into the XbaI and BamHI sites of the p3xFLAG-Myc-CMV vector (Sigma). The mutants were constructed by primers harboring the desired mutations through site-directed mutagenesis. PCR amplification performed by KOD DNA Polymerase (Toyobo) using specific PCR primers are provided in key resources table. Plasmids were transfected into HEP-2 or 293T cells using Lipofectamine 2000 (Invitrogen) following the manufacturer's instructions.

Western blotting

3×10^5 human HEP-2 cells were seeded on 3.5-cm culture dishes and incubated overnight. Culture medium was replaced with conditional medium for the indicated times. Total protein was extracted from the cells with RIPA buffer (50 mM Tris-HCl [pH 7.2], 150 mM NaCl, 2mM EDTA, 1% NP40, 0.1% SDS, 1% sodium deoxycholate) and 1X protease inhibitor cocktail (Complete Mini, Roche). Cells were washed with ice-cold PBS and collected in RIPA buffer with protease inhibitors, followed by incubation on ice for 30 min. The protein concentration was measured using the Bradford method (Protein Assay, Bio-Rad). Twenty micrograms of protein was loaded per well, subjected to SDS-PAGE, and transferred to PVDF membranes. Membranes were blocked with 5% nonfat milk in TBS-T (0.1% Tween 20 in Tris-buffered saline) for 1 h and incubated overnight at 4°C with primary antibodies diluted 1:1000 in 5% nonfat milk in TBS-T buffer, washed 3 times in TBS-T followed by incubation of secondary antibodies for 1 h. Membranes were developed using ECL (PerkinElmer), specific bands were detected on a transilluminator (UVP) and quantified by densitometry.

Cell growth and bromodeoxyuridine (BrdU) incorporation assays

10^5 HEP-2 cells were seeded overnight and incubated with EBSS and EBSS + His for 48 h, then replaced by DMEM for 24 and 48 h. The numbers of cell were counted at indicated time points. For BrdU incorporation assay, treated cells were incubated in media containing 30 μ g/ml BrdU for 1 h. Cells were fixed in 4% formaldehyde in PBS (pH 7.4) for 10 min at room temperature. Following by washing in PBS for 3 times, cells were permeabilized in PBST (0.2% Triton in PBS) for 10 min. The cells were incubated in 2N HCl for 20 min, followed by washing in PBS (pH 8.5) for 3 times. For BrdU immunostaining, cells were blocked in 1% BSA in PBS for 30 min, followed by incubation of anti-BrdU antibodies (1:50) at 4°C overnight. After washing in PBS, incubated with Alexa Fluor 488 goat anti-mouse secondary antibodies (1:500).

Recombinant lentivirus shRNA gene knockdown

The lentivirus based shRNA knockdown system was provided by the National RNAi Core Facility, Academia Sinica. The target sequences for specific genes are provided in key resources table. The cells were infected with 9×10^5 CFU/ml recombinant viral fluid in the presence of 8 μ g/ml polybrene (Sigma-Aldrich) for 24 h. Infected cells were washed with PBS and grown in fresh DMEM for 24 h, followed by selection in 2 μ g/ml puromycin (Invivogen) for one week. Puromycin resistant cells were collected for experimental analysis.

Gene expression

Total RNA was isolated from cells using TRIzol Reagent (Thermo Fisher Scientific). 5 μ g of total RNA and random hexamer were used to perform reverse transcription with RevertAid First Strand cDNA Synthesis Kit (Thermo Fisher Scientific). Specific PCR primers used for PCR amplification are provided in key resources table. Real-time PCR amplification was performed using specific primers and Power SYBR Green PCR Master Mix (Thermo Fisher Scientific) in a StepOnePlus instrument (Thermo Fisher Scientific). Relative expression of target genes was obtained by normalization of GAPDH. Statistical analyses were performed by Student's t test.

Intracellular ROS measurement

1×10^5 Cells were incubated in DMEM or glutamine/serum-free medium for 24 h. After 24 h, cells were treated with 5 μ M dichloro-dihydrofluorescein diacetate (DCF-DA, Invitrogen) for 30 min at 37°C. Cells were harvested and washed twice with PBS. Data were acquired and analyzed using flow cytometry (BD Bioscience).

Protein structure modeling

The R294 and R449 residues were fit to cryo-EM map of hCTPS1 filament (EMD-8474; PDB 5U03) using CHIMERA ([Lynch et al., 2017](#); [Pettersen et al., 2004](#)).

Measurement of intracellular amino acids

The cell protein were precipitated by adding 1ml of 80% methanol, supernatants were dried with nitrogen gas. Sample were redissolved with 100 μ L water, and 16 μ L sample combined with 4 μ L internal standard (norvaline 250 μ M), 60 μ L working buffer (borate buffer, pH 8.8). The derivatization was initiated by addition of 20 μ L of 10 mM AQC in acetonitrile. After 10 minutes incubation, sample were analyzed using the ACQUITY UPLC System. AQC derivatization reagent was obtained from Waters Corporation (Milford, MA, USA) ([Pappa-Louisi et al., 2007](#)). The Waters ACQUITY UPLC® System consisted of a Binary Solvent Manager, a Sample Manager fitted with a 10 μ L loop, and a Photodiode Array (PDA) Detector. The system was controlled and data collected using Empower 2 Software. Separations were performed on a 2.1 \times 100 mm ACQUITY BEH C18 column at a flow rate of 0.6 mL/min. Column

temperature was set at 55°C and injection volumes for all samples and standards were 2 μ L. Analytes were eluted from the column using with a linear gradient: 0–2.5 min: 0.1% B; 2.5–3.2 min: 0.1%–2% B; 3.2–3.9 min: 2%–9% B; 3.9–4.5 min: 9%–10% B, keep 0.9 min; 5.4–6.5 min: 10%–20% B; 6.5–7.74 min: 20%–21.2% B; 7.74–8.05 min: 21.2%–90% B, keep 0.6 min; and 1 min for re-equilibration. The mobile phase was 20 mM ammonium formate/ 0.6% formic acid/ 1% acetonitrile in water (Eluent A) and acetonitrile (Eluent B). Detection was set at 260 nm using a sampling rate of 20 points per second.

Detection of CTPS1 methylation sites

For identifying histidine induced protein methylation sites on CTPS1, critical for filament assembly, quantitative analysis of CTPS1 methylation was performed using LC-MS-MS approach. CTPS1 was tagged using an ascorbate peroxidase, APEX2, which utilizes biotin phenol and hydrogen peroxide (H_2O_2) to produce very short-lived biotin-phenoxy radicals which can label any protein near the APEX2 protein. CTPS1 was cloned into the NotI and BamHI sites of p3xFlag-Myc-CMV26 vector. APEX2 was amplified from APEX2 - Actin in pEGFP (a gift from Alice Ting [Addgene plasmid # 66172]) (Lam et al., 2015) was cloned into the BamHI site of p3xFlag-CTPS1-CMV26. Cells transfected with Flag-CTPS1-APEX2 were subjected to three conditions “EBSS,” “EBSS + His” (200 μ M Histidine was added to the medium) and “EBSS + His + Gln” (4 mM glutamine was added to the medium during the last 15 mins of incubation) whereas those transfected with Flag-APEX2 alone were subject to only the “EBSS + His” condition. After incubation in the conditional medium for 6 h, each group was incubated with 500 μ M biotin phenol for 30 min in their respective media. For initiating the reaction, 1 mM of H_2O_2 was added to the cells for 1 min and the reaction then quenched using quencher solution containing 10 mM sodium ascorbate, 10 mM sodium azide, and 5 mM Trolox. Cells were lysed with denaturing buffer (1% SDS, 50 mM Tris-HCl [pH 7.4], and 5 mM EDTA) at room temperature and then diluted with non-denaturing buffer (1% Triton X-100, 50 mM Tris-HCl [pH 7.4], 300 mM NaCl and 5 mM EDTA) to reduce the SDS concentration to 0.1% as required for IP experiments. Biotinylated proteins were pulled down using streptavidin coated magnetic beads and subjected to quantitative LC-MS-MS analysis. The details of the approach have been previously published (Hung et al., 2016). Streptavidin-pull-down products were eluted with 0.1% trifluoroacetic acid (TFA) / 50% acetonitrile (ACN) and dried in a Speed-Vac followed by in-solution digestion. Briefly, samples were dissolved in 250 mM triethylammonium bicarbonate (TEABC) (Sigma-Aldrich, St. Louis, MO, USA), reduced with 5 mM Tris(2-carboxyethyl) phosphine (TCEP) (Sigma-Aldrich) for 1 h at 60°C, alkylated with 10 mM methyl methanethiosulfonate (MMTS) (Sigma-Aldrich) at room temperature for 30 min, and subsequently digested with sequencing grade modified porcine trypsin (20 μ g/mL; Promega, Madison, WI, USA) overnight at 37°C. The resulting tryptic peptides were dried by Speed-Vac, dissolved in 50 mM TEABC and then labeled with iTRAQ reagent (Applied Biosystems, Foster City, CA, USA) for 1 h at room temperature. All labeled peptides were mixed at a 1:1:1 ratio and desalted using a homemade C18 microcolumn for subsequent two-dimensional liquid chromatography-tandem mass spectrometry (2DLC-MS/MS) analysis. The peptide mixtures were separated and analyzed by 2DLC-MS/MS using a strong cation exchange (SCX) and reverse-phase C18 (RP18) liquid chromatography system coupled to a LTQ-Orbitrap Elite mass spectrometer (Thermo-Fisher Scientific, Waltham, MA, USA). The peptide mixture was reconstituted in HPLC buffer A (30% acetonitrile/0.1% formic acid) and loaded onto a homemade column (Luna SCX, bead size, 5 μ m; column dimensions, 180 \times 0.5 mm) (Phenomenex Inc., Torrance, CA, USA) at flow rate of 5 μ L/min for 30 minutes. The peptides were then fractionated into 44 fractions using a continuous HPLC buffer B gradient (0%–100% of 0.5 M ammonium chloride in the presence of 30% acetonitrile/0.1% formic acid). Each fraction was then mixed with a stream of 0.1% FA/ H_2O and the peptides trapped on a Zorbax C18 column (bead size, 5 μ m; pore size, 30 nm; column dimensions, 5 \times 0.3 mm) (Agilent Technologies Inc., Santa Clara, CA, USA) and separated by Hydro RP column (bead size, 2.5 μ m; pore size, 10 nm; column dimensions, 200 \times 0.075 mm) (Phenomenex Inc.) chromatography using a linear gradient of 3%–28% HPLC buffer C (99.9% acetonitrile/0.1% formic acid) for 37 min, 28%–50% buffer C for 12 min, 50%–95% buffer C for 2 min, 95% buffer C for 5 min, and 3% buffer C for 9 min with a flow rate of 0.3 μ L/min on a Dionex UltiMate 3000 nano LC system (Thermo-Fisher Scientific). MS/MS analysis was performed on a LTQ-Orbitrap Elite mass spectrometer. Full-scan MS spectra (m/z 400 - m/z 2000) were acquired on the mass analyzer at a resolution of 60,000 at m/z 400, followed by MS/MS of the six most intense precursor ions, above a threshold of 5,000, selected for fragmentation by collision induced dissociation (CID) and high-energy collision dissociation (HCD) in parallel acquisition mode with a normalized collision energy setting of 35% and an activation time of 10 ms for CID and 0.1 ms for HCD. The dynamic exclusion function was set as: repeat count, 1; repeat duration, 30 s; and exclusion duration, 40 s. The MS and MS/MS data were analyzed and quantified using Proteome Discover (version 1.4) (Thermo-Fisher Scientific) against the Swiss-Prot database (download in September 2015; *Homo sapiens*; containing 20,205 entries). Mass tolerance for parent and fragment ions was set to 10 ppm and 0.5 Da for CID and 10 ppm and 0.05 Da for HCD. Two missed cleavages were allowed for trypsin digestion; methylation of cysteine was set as a fixed modification, and oxidation of methionine, protein N-terminal acetylation, pyroglutamination for N-terminal glutamine, iTRAQ labeling of lysine, and N terminus of peptides were set as variable modifications for protein identification; additionally, methylation of arginine, dimethylation of lysine and arginine, and trimethylation of lysine were added for methylated peptide identification. The criteria for peptide identification were as follows: peptide confidence, high; peptide length, 7–100; peptide maximum rank, 1; search engine rank, 1; minimal number of peptides, 1 for methylated peptides and 2 for proteins; count only rank 1 peptide; count peptides only in top-scoring proteins; and FDR < 0.01.

Untargeted metabolite analysis

4×10^6 HEp-2 cells were seeded and incubated overnight, followed by incubation with DMEM, EBSS, or EBSS + His for 4 h. Cells were extracted as previously described with modifications (Munger et al., 2006). The medium was aspirated from the culture plates and the plates washed at least twice with PBS. Following washing, 1 mL cold 80% methanol was immediately added to quench metabolic activity and extract the metabolites. Cells were then scraped from the culture dish on ice and centrifuged at 12,000 rpm for 10 min at 4°C. The supernatants were transferred into clean tubes and dried under N₂. The dry sample was dissolved in 100 μ L water containing 0.1% formic acid for analysis. Metabolites were separated on an ACQUITY HSST3 C18 (2.1 \times 100 mm, 1.7 μ m) column at 40°C using linear gradients at a flow rate of 0.4 mL/min: 0–4 min, 1%–50% B; 4–5 min, 50%–98% B; 5–7.4 min, 98% B; 7.4–10 min, 1% B for re-equilibration. The mobile phase consisted of 0.1% formic acid in water (solvent A) and 0.1% formic acid in acetonitrile (solvent B). Each sample was analyzed in triplicate. Mass spectrometry was performed on a Waters Q TOFMS (SYNAPT G1 HDMS, Waters MS Technologies, Manchester, UK) operating in positive ion modes. The desolvation gas was set to 700 L/h at a temperature of 400°C and the cone gas 25 L/h, the source temperature was 100°C. The capillary and cone voltages were set to 3,000 and 35 V, respectively. Sulfadimethoxine was used as the lock mass standard (an [M+H]⁺ ion at 311.081 Da in ESI positive mode). QC samples were prepared from mixed samples and analyzed during the analytical runs after every 15th sample. Raw mass spectrometric data were processed using MassLynx V4.1 (Waters Corp., Milford, USA). The intensity of each mass ion was normalized with respect to the total ion count to generate a data matrix that included the retention time, m/z value, and normalized peak area.

Targeted metabolite analysis

Samples were subjected to ultrahigh performance liquid chromatography coupled with triple quadrupole mass spectrometry (Waters corp.) Targeted metabolites were analyzed using a modified method as previously described (Chou et al., 2014). Single analyte standards dissolved in a mixture of water/methanol 50:50 (v/v) were infused for tuning purposes. Major MS/MS fragment patterns of each analyte were determined. The optimized parameters were as follows: capillary voltage 2 kV in positive mode; desolvation temperature 300°C; source temperature 150°C; desolvation gas flow 800 L/h; and cone gas flow 150 L/h. Chromatographic separation was achieved on an ACQUITY HSST3 C18 column (150 \times 2.1 mm, particle size of 1.7 μ m; Waters Corp., Milford, USA) at 40°C with elute A (0.1% formic acid in water) and eluent B (0.1% formic acid in acetonitrile) at a flow rate of 0.4 mL/min. The gradient profile was as follows: 0–2 min, isogradient 1% B; 2–5 min linear gradient 1%–40% B; 5–5.2 min, linear gradient 40%–98% B, 0; and 5.2–7.2 min 98% B. The column was then re-equilibrated for 3 min. Results were analyzed using Targetlynx 4.1 software systems (Waters Corp., Milford, USA). The UPLC/TQMS analysis was conducted in the Metabolomics Core Laboratory of the Healthy Aging Research Center, Chang Gung University.

Dansylation labeling and LC-MS analysis

1.5×10^6 cells were harvested and small molecules were extracted by methanol. Supernatants were dried and re-suspended in 50 μ L water, and then labeled by dansyl chloride. Dansylation method was based on Guo's study (Guo and Li, 2009). 25 μ L of 0.5 M NaHCO₃/Na₂CO₃ and 75 μ L of dansyl chloride (1mg in 80.5 μ L of acetonitrile) were added into 50 μ L samples. The solution were reacted in an orbital shaker incubator at 200 rpm at 40°C for 45 min, and immediately moved on ice to stop the reaction. Excess dansyl chloride was quenched by 10 μ L of 250 mM NaOH and incubated at 40°C for 10 min. 50 μ L of 425 mM formic acid /50% acetonitrile was added into the samples for LC-MS analysis. Four micro liter labeled samples were analyzed by Bruker Impact II QTOF mass spectrometer (Bruker Daltonics, Bremen, Germany) linked to a Agilent 1290 series binary HPLC system (Palo Alto, CA, USA) connected with a reversed-phase Waters ACQUITY BEH C18 column (1 X 100 mm, 1.7 mm particle size, 130 Å). Solvent A was 0.1% (v/v) formic acid in water, and solvent B was 0.1% (v/v) formic acid in acetonitrile. The gradient elution conditions were: t = 0 min, 5% B; t = 2 min, 5% B; t = 3 min, 15% B; t = 13 min, 35% B; t = 25 min, 70% B; t = 28 min, 99% B; t = 30 min, 99% B; t = 30.1 min, 5% B; t = 32.5 min, 5% B. The flow rate was 60 μ L/min. All MS spectra were obtained in the positive ion mode. The peak area of dansylated-¹²C-Methionine and ¹³C-Methionine the raw LC-MS data were analyzed using Bruker Compass DataAnalysis 4.3 software. (Bruker Daltonics, Bremen, Germany).

Measurement of labeling UTP and CTP

1.5×10^6 cells were harvested by methanol. Supernatants were dried and re-suspended in 2 mM Dibutylamine and 1.5 mM Formic acid. Extracts of 10^4 cells were analyzed by LC-MS (LTQ-orbitrap, Thermo) linked to a Waters ACQUITY UPLC system (Waters, Milford, MA, USA) connected with Luna omega (2.1 X 100 mm, 1.6 μ m particle size, 100 Å). The flow rate is 60 μ L/min and solvent A was 2 mM Dibutylamine and 1.5 mM Formic acid in water, and solvent B was Methanol. The gradient elution conditions were: t = 0 min, 1% B; t = 0.5 min, 1% B; t = 11 min, 30% B; t = 14 min, 99% B; t = 19 min, 99% B; t = 20 min, 1% B; t = 25 min, 1% B. All MS spectra were obtained in the negative ion mode. The peak area of ¹²C-CTP/UTP and ¹³C-CTP/UTP from the raw LC-MS data were analyzed using Thermo Xcalibur Qual Browser 2.2 software (Thermo) (Klawitter et al., 2007).

Progression-free survival analysis

Survival clinical information and expression levels for HNSC, ESCA, STAD, LIHC, PAAD, CHOL, CRC, BRCA, LUAD, LUSC, PRAD and BLCA were downloaded with R package curatedTCGADData (Clinical data: ver. 1.5.0 (Mar.2016)). Log-ranked p value and plot in survival analysis were from GraphPad Prism software.

QUANTIFICATION AND STATISTICAL ANALYSIS

Experimental data were analyzed by Student's two-tailed unpaired *t* test using GraphPad Prism software. All statistical details of experiments are included in the figure legends.

DATA AND SOFTWARE AVAILABILITY

Microarray analysis

HEp-2 cells were cultured in DMEM, EBSS and EBSS + His for 4 h. Total RNA was extracted by Trizol, followed by concentration through an RNeasy MinElute Cleanup Kit (QIAGEN), following the manufacturer's instructions. Isolated RNAs were subjected to GeneChip Human Transcriptome Array 2.0 analysis. The accession number for the data reported in this paper is GEO: GSE105251.